Dissolution kinetics of zinc oxide and its relationship with physicochemical characteristics

Denise Cardoso, Agnès Narcy, Stéphane Durosoy, Claire Bordes, Yves Chevalier

DISSOLUTION KINETICS OF ZINC OXIDE AND ITS RELATIONSHIP WITH PHYSICOCHEMICAL CHARACTERISTICS

Denise Cardoso,[a,b,c] Agnès Narcy,[b] Stéphane Durosoy,[c] Claire Bordes,[a] Yves Chevalier [a,*]

[a] University of Lyon, *LAGEPP, CNRS UMR 5007, Université Lyon 1, 43 bd 11 Novembre, 69622 Villeurbanne, France.*

[b] INRA, *UR 83 Recherches Avicoles, 37380 Nouzilly, France.*

[c] Animine, *10 rue Léon Rey-Grange, 74960 Annecy, France.*

* Corresponding author

E-mail addresses: dcardoso@animine.eu (D. Cardoso), agnes.narcy@inra.fr (A. Narcy), sdurosoy@animine.eu (S. Durosoy), claire.bordes@univ-lyon1.fr (C. Bordes), yves.chevalier@univ-lyon1.fr (Y. Chevalier).

Highlights

- Discrimination of reaction-limited and diffusion-limited dissolution is done from the dependence on physicochemical parameters
- Variability in ZnO dissolution kinetics is accounted for through statistical analysis
- Dissolution kinetics of coarse ZnO powders depends on specific surface area
- Dissolution kinetics of fine ZnO powders depends on aggregation and agglomeration

ABSTRACT

Dissolution kinetics of zinc oxide (ZnO) powders used as feed additives for supplementation in diet of animals is studied in relation to the powder physicochemical characteristics. The fundamental issue of discrimination of reaction-limited or diffusion-limited dissolution into a stirred liquid medium is addressed. Relationships between dissolution kinetics and physicochemical properties are investigated for a set of 34 ZnO samples of various origins. A principal component analysis allows sorting ZnO samples in three clusters having different physicochemical properties. A correlation analysis discloses the most relevant physicochemical characteristics affecting dissolution: density, agglomerate size and specific surface area. Coarse particles dissolve in a reaction-limited process according to their specific surface area. Fine aggregated particles dissolve in 2 steps: reaction-limited dissolution at the surface of ZnO primary particles, followed by diffusion in the quiescent liquid medium between primary particles to the stirred bulk aqueous medium. A reaction-diffusion model is proposed.

Keywords: dissolution kinetics; zinc oxide; physicochemical characterization; bioavailability; diffusion

Abbreviations

ZnO: zinc oxide; PCA: principal component analysis; HAC: hierarchical ascendant clustering; SAP: small aggregated particles; SAAP: small aggregates and agglomerated particles; LDP: large dense particles.

1. Introduction

Dissolution kinetics of a solid powder is one parameter that affects bioavailability. This is of relevance in many areas such as drug delivery, and human food or animal feed digestion. Indeed, the bioavailable part is that in solution in the gastrointestinal fluid or in the blood stream. Obviously bioavailability requires that dissolution is faster than the residence time in the body. As example, cellulose fibers cannot be digested by humans although cellulose is slowly digested by microorganisms in the soil for the production of humus.

Such general issue is presently investigated in the scope of zinc supplementation of animal feed using zinc oxide (ZnO). In cereal-based feed of monogastric animals, zinc is a limiting ingredient that is often supplemented in diets [1,2,3,4,5]. The most common sources of zinc used in supplementation of animal feeding are the 'soluble forms' zinc sulfate and zinc chelates, and solid powder of zinc oxide. There is a poor characterization of supplemented sources; they are most often just differentiated by their solubility in water that is thought being related to their bioavailability. However, studies comparing *in vitro* solubility and *in vivo* digestibility of minerals have shown a negative correlation [6]. Although ZnO is claimed not soluble in water, this mineral is highly soluble as Zn^{2+} ions in gastric conditions where pH ranges from 2 to 4 [7]. The literature reports a variability of ZnO bioavailability among the different sources of ZnO from 30 to 105% of the zinc sulfate reference compound [5,8]. Bioavailability of ZnO involves several complex phenomena; one of these being the kinetics of dissolution.

The present works addresses fundamental issues related to physicochemical processes involved in dissolution kinetics. Thus, dissolution process in a stirred liquid medium can be split into two successive steps: dissolution itself at the surface of the solid, followed by diffusion to the bulk

solution inside the quiescent medium close to the surface. The first question that arises is as which of the two steps is rate-determining.

It is often considered that dissolution is controlled by the diffusion step because the first step of dissolution is very fast. Then, the solid is in equilibrium with a saturated solution in contact to its surface. The concentration gradient entering the first Fick's law is the difference of the saturation concentration (solubility) and the bulk concentration in the stirred liquid medium ($C_S - C$).

Dissolution itself can be quite slow. This may be the case of ZnO since its dissolution is a hydrolysis reaction that converts ZnO into Zn^{2+} ions in solution. Chemical reactions are often slow. Chemical kinetics is characterized by rate constants for molecule release into solution (k_-) and integration into the solid (k_+). The concentration that matters is that of the solution close to the solid surface (C_{surf}).

The general form of kinetics equations for both steps is the same. For a diffusion-limited dissolution, the flux to the bulk solution is

$$J = -\frac{1}{A}\frac{\mathrm{d}n}{\mathrm{d}t} = k_\mathrm{d}(C_\mathrm{S} - C) \qquad (1)$$

where the factor k_d contains contributions from the several parameters influencing diffusion.

For a reaction-limited process, it is

$$J = -\frac{1}{A}\frac{\mathrm{d}n}{\mathrm{d}t} = k_- - k_+ C_\mathrm{surf} = k_- - k_+ C \qquad (2)$$

Since $C_{surf} = C_S$ at equilibrium, $k_- - k_+ C_s = 0$, and Eq. (2) takes the form given by Berthoud as [9]

$$J = k_+(C_\mathrm{S} - C) \qquad (3)$$

These simple considerations show that discrimination of the two processes is not possible on the sole basis of the kinetic profile. Discrimination of reaction and diffusion is presently achieved by looking at the influence of physicochemical parameters of the solid because their influence on

either the reaction or the diffusion step is known to some extent. This is a difficult task because many physicochemical parameters of the solid material contribute to the two elementary steps and neither their values nor their exact roles are known with accuracy.

As there are many parameters and they are cross-correlated, the strategy of this study was to firstly characterize and categorize samples of ZnO used in animal feeding, and further investigate the influence of the relevant parameters on the dissolution rate, so as to propose a mechanistic model in a third stage.

A set of 34 samples of ZnO was collected from the feed industry in Europe, Asia and Americas. Samples were analyzed for crystal size and shape, particle size, aggregation and agglomeration, specific surface area (A_{sp}), bulk density and tapped density. A Principal Component Analysis (PCA) allowed clustering samples into families, according to their characteristics. Dissolution kinetics of ZnO samples was studied, so as to disclose the parameters influencing dissolution through a statistical analysis.

2. Experimental section

2.1. Physicochemical characterization

X-Ray Diffraction

Crystallographic and crystal size information on zinc oxide samples were obtained using a Bruker AXS D8 Advance diffractometer at the 'Centre de Diffractométrie Henri Longchambon' facility of the University Lyon 1 (http://cdalpha.univ-lyon1.fr/), operating in the Bragg θ-2θ configuration using Cu Kα radiation (0.154 nm wavelength) provided Debye–Scherrer X-ray diffraction powder patterns in an angular domain from 10 ° to 70 ° at scanning rates of 0.25 °min^{-1}.

Transmission Electron Microscopy (TEM)

Size and shape of structures were determined by TEM analysis, with images taken at an acceleration voltage of 80 kV on a Philips CM120 instrument at 'Centre Technologique des Microstructures' facility of the University of Lyon 1 (http://microscopies.univ-lyon1.fr/). Specimens for all TEM experiments were prepared by dispersing particles in water (0.1 %) by sonication for 1 min at 50% amplitude with a Hielscher UP400S ultrasound device. 5 µL of the dispersion was spread on Formvar/carbon grids and dried before observation.

Scanning Electron Microscopy (SEM)

Size and shape were complementary determined by SEM. The images were taken at 'Centre Technologique des Microstructures' – University of Lyon using a FEI Quanta FEG 250 instrument working at an acceleration voltage of 10 kV. Samples were prepared by casting a thin layer of ZnO powder on a conductive carbon paste tape stuck to aluminum stubs, followed by metallization with a 10 nm thick deposit of copper.

Particle Size

The diameter of ZnO aggregates and agglomerates in water was measured by low-angle laser light scattering using a Malvern Mastersizer 3000 instrument. Agglomerate and aggregate size distributions were calculated from Mie theory using the refractive indices of water (1.33) and ZnO (2.004) and absorption index (imaginary part of complex refractive index) of ZnO of 0. Agglomerates were assessed by directly adding the dry ZnO powder in the water under mild stirring with a magnetic stir bar. Measurements of aggregate sizes implemented a powerful dispersion of ZnO at a concentration of 10% using an IKA Ultra-Turrax Rotor-Stator device rotating at 15,000 rpm for 15 min that could break up agglomerates. Mean size was expressed as the median diameter $D(0.5)$ of the particle size distribution.

Specific Surface Area

Specific surface area (A_{sp}) of dry powders was measured by nitrogen adsorption experiments using a Micromeritics Tristar 3000 BET instrument. A_{sp} was determined by the Brunauer–Emmet–Teller (BET) multipoint method using data at relative pressures between 0.05 and 0.3. The porosity was calculated from the desorption branch above 0.4 relative pressure by the Barrett–Joyner–Halenda (BJH) method.

Bulk density and Tapped density

40 g of dry ZnO powder was poured into a graduated cylinder for its volume to be measured. Bulk density is defined as mass over volume. The shortcut "density" was used throughout the paper.

Tapped density was measured using a Tapped Density Tester series JV from Copley Scientific according to the ISO 8398 standard (1989). The final volume was noted after 250 ± 15 tapings and tapped density was calculated as mass over tapped volume.

Dissolution kinetics

Kinetics was assessed at 40 °C with 0.15 g of ZnO in 200 mL of deionized water at pH 4 kept constant. The liquid medium contained in a beaker of 70 mm diameter was stirred with a three blades marine propeller of 30 mm diameter rotating at 625 rpm. Hydrochloric acid (HCl 1 M) was added using an automatic burette (877 Titrino plus, Metrohm) for keeping pH at the constant value of 4 while ZnO was dissolving. The volume of HCl supply was recorded during the experiment, providing kinetics of base release coming from dissolution. In addition, samples were collected at different times, centrifuged for 5 min at 14,000 rpm. 100 µL of supernatant of each sample was diluted in 10 mL of deionized water for ICP-OES analysis of Zn using a Thermo Scientific™ iCAP™ 7000 with detection at 213.857 nm wavelength.

2.2. Multivariate Statistical Analysis

Multivariate data analyses were performed using XLSTAT software (Addinsoft, www.xlstat.com).

Principal Component Analysis (PCA)

A Principal Component Analysis (PCA) was performed to observe if ZnO samples belong to groups (classes) according to their physicochemical properties.

PCA aims at reducing the dimensionality of the dataset by building a new coordinate space of Principal Components (PC's) made up of linear combinations of the initial variables. PC's were calculated so as to account for most of the variance in the dataset [10,11]. PCA calculations were performed using standardized initial variables so as to give them equal statistical weight in the analysis.

Hierarchical Ascendant Clustering (HAC)

HAC is a clustering method based on an agglomerative (bottom up) approach which initially considers each sample as a cluster. Pairs of clusters are hierarchically put together by using the Ward's linkage criterion based on the Euclidian distance metric that seeks minimizing intra-cluster variance while maximizing inter-cluster one [12,13]. These successive clustering operations allow obtaining a clustering tree called dendrogram.

Correlation analysis

An analysis of correlation between properties analyzed and zinc concentration at 10 min and 20 min was considered to assess which factors have a significant influence on dissolution kinetics. The matrix of Pearson's correlation coefficients (R) was determined for the whole dataset. A t-test was done to evaluate significance of differences between different dissolution behaviors.

3. Results and Discussion

3.1. Physicochemical characterization

Differentiation between feed grade zinc oxides is often based on purity, chemical composition, specific surface area, and manufacturing process [14]. Dry powders consist of a complex assembly of crystals, known as primary particles, associated in the form of aggregates and/or agglomerates [15]. Aggregates and agglomerates behave as large particles with internal porosity [16]. Aggregates cannot be broken into primary particles by common mechanical means, whereas agglomerates can be broken into aggregates [17,15,16]. In this framework, the 'size' of particles is defined by the three sizes of primary particles, aggregates and agglomerates.

Physicochemical characterization of ZnO dry powders and aqueous suspensions was performed using X-ray diffraction (XRD), transmission (TEM) and scanning (SEM) electron microscopy, small-angle light scattering, bulk and tapped density, and BET determination of specific area (A_{sp}). Detailed presentations of measurements and their outcomes are reported in the Supplementary Material file. All ZnO samples were made of crystalline zincite, which is the only known crystalline structure of ZnO. The size of the smallest primary particles could be assessed from the width of the XRD reflections. But the angular resolution of XRD prevented the size determination of large crystals (> 100 nm). Image analysis of TEM or SEM pictures also failed to that end. The specific area was taken as a measurement of primary particle size. Light scattering allowed the determination of both aggregates and agglomerates sizes: agglomerates were obtained by a mild dispersion of ZnO powder in water, and aggregates were generated by a powerful dispersion that

broke agglomerates. The ratio of agglomerates to aggregates sizes was called ‘agglomeration ratio’. The full results are given in Table 1.

Table 1. Physicochemical properties of ZnO samples.

Sample	Shape of primary particles	Size of crystallites (nm)	Aggregate *D*(0.5) (μm)	Agglomerate *D*(0.5) (μm)	Agglomeration ratio	Density ($g \cdot cm^{-3}$)	Tapped density ($g \cdot cm^{-3}$)	Hausner ratio	A_{sp} ($m^2 \cdot g^{-1}$)
ZnO-1	Platelet	24	4.6	117	35.0	0.93	0.98	1.05	37.0
ZnO-2	Platelet	26	5.5	111	52.3	0.95	1.03	1.08	25.9
ZnO-3	Platelet	24	5.6	118	46.2	1.00	1.05	1.05	31.6
ZnO-4	Platelet	22	6.4	158	54.7	1.00	1.08	1.08	38.0
ZnO-5	Platelet	> 100	18.0	22.7	12.3	2.01	2.36	1.18	0.5
ZnO-6	Platelet	> 100	27.6	43.6	23.4	2.35	2.58	1.10	0.3
ZnO-7	Platelet	> 100	16.8	28.2	13.7	2.23	2.51	1.12	0.3
ZnO-8	Sphere	39	8.3	26.6	14.0	1.00	1.25	1.25	19.4
ZnO-9	Platelet	25	9.6	12.0	6.3	0.78	1.08	1.38	18.7
ZnO-10	Platelet	28	14.4	13.5	8.1	0.40	0.49	1.21	28.1
ZnO-11	Platelet	34	8.7	8.7	5.6	0.76	1.05	1.40	7.2
ZnO-12	Platelet	27	7.7	14.4	7.9	0.56	0.73	1.29	26.5
ZnO-13	Rod-like	> 100	7.0	39.4	19.3	0.60	0.73	1.22	2.6
ZnO-14	Rod-like	> 100	5.6	33.8	22.9	0.66	0.76	1.15	4.3
ZnO-15	Rod-like	> 100	7.2	129	64.8	0.78	0.87	1.11	2.4
ZnO-16	Rod-like	> 100	5.4	45.8	30.0	0.70	0.80	1.14	5.1
ZnO-17	Rod-like	> 100	5.9	75.7	45.5	1.00	1.11	1.11	6.3
ZnO-18	Rod-like	> 100	3.8	8.8	2.6	0.46	0.58	1.26	4.2
ZnO-19	Rod-like	> 100	5.8	5.6	2.5	0.80	0.98	1.22	2.0
ZnO-20	Platelet	> 100	17.9	36.6	23.7	2.00	2.22	1.11	0.0
ZnO-21	Rod-like	> 100	4.7	7.0	4.6	0.64	0.74	1.17	4.7
ZnO-22	Rod-like	> 100	5.8	4.7	2.3	0.51	0.63	1.24	2.9
ZnO-23	Rod-like	> 100	3.6	39.4	23.2	0.48	0.59	1.24	13.1
ZnO-24	Rod-like	> 100	5.4	4.0	2.7	0.56	0.65	1.14	4.4
ZnO-25	Rod-like	36	4.0	15.8	6.9	0.68	0.87	1.28	16.8
ZnO-26	Rod-like	56	4.2	32.7	24.6	0.28	0.34	1.19	12.6

ZnO-27	Platelet	23	5.5	12.8	6.1	0.46	0.63	1.38	29.0
ZnO-28	Platelet	18	5.3	25.6	8.2	1.13	1.23	1.09	41.0
ZnO-29	Rod-like	69	15.0	25.8	13.2	2.35	2.67	1.13	0.2
ZnO-30	Platelet	57	12.9	23.7	10.6	2.22	2.50	1.13	0.1
ZnO-31	Platelet	93	6.6	35.1	15.9	2.50	2.67	1.07	0.1
ZnO-32	Platelet	25	5.4	9.1	5.1	0.69	0.82	1.18	21.2
ZnO-33	Platelet	59	24.3	44.6	18.0	2.51	2.87	1.14	0.4
ZnO-34	Platelet	21	4.7	5.8	3.4	0.67	0.80	1.20	35.9

Electron microscopy pictures of samples allowed sorting ZnO samples into 4 different groups corresponding to types of Fig. 1A,B,C,D. This classification relying on pictures provides rather subjective pieces of information. Several samples presented a bimodal population as observed on SEM pictures (Fig. 1). Others presented a homogeneous unimodal size distribution of small primary particles, though the latter were associated into large agglomerated structures. So as to reach a classification of ZnO particles in terms of their physicochemical properties that is free of subjectivity, a rigorous statistical analysis was performed using PCA.

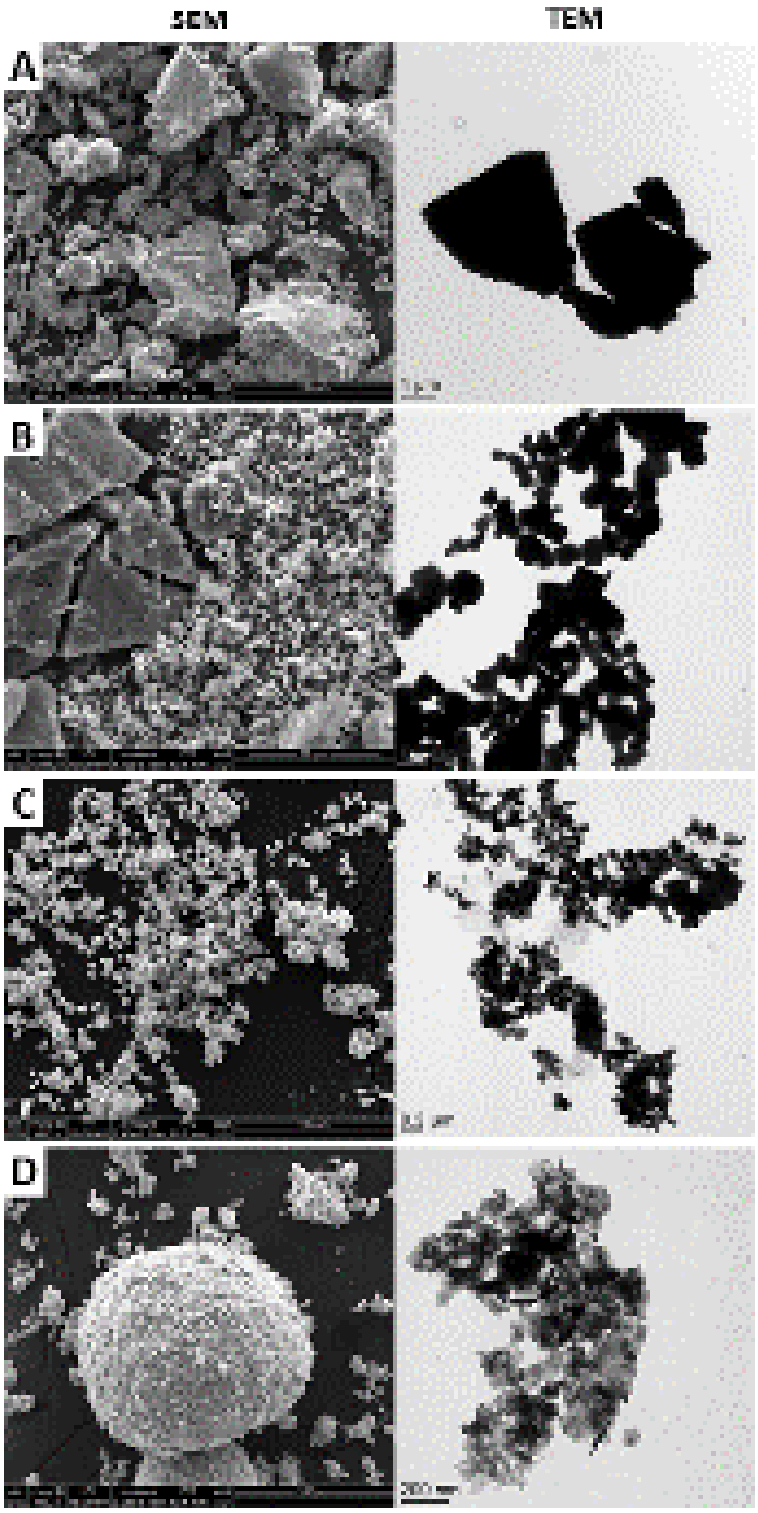

Figure 1. Typical electron microscopy pictures of ZnO powders. SEM (left) and TEM (right) show the main structures of different powders. Pictures A, B, C and D correspond to ZnO-6, ZnO-21, ZnO-12 and ZnO-4 in Table 1.

3.2. Classification of ZnO grades with respect to their physicochemical properties

PCA was firstly used to represent ZnO samples in a low-dimensional space. The purpose was to categorize ZnO grades in terms of their physicochemical characteristics, to identify which properties are characteristic of each family, and to select one representative sample in each family for further studies.

The raw dataset (Table 1) contains 34 samples in the 7-dimensional space of the 7 physicochemical parameters that could be measured for the whole set of samples: Specific surface area, aggregate median diameter, agglomerate median diameter, agglomeration ratio, powder density, tapped density and Hausner ratio. The physicochemical parameters were reduced in standardized form by rescaling them with both their average value and standard deviation for each parameter for they contribute with the same weight in the PCA analysis. The number of variables needs being reduced to those of highest relevance, that is, with the highest contribution to the variance. The samples were placed in a lower-dimensional space by applying a PCA to the dataset.

The projections of physicochemical parameters onto the plane defined by the first two Principal Components (PC's) contributing the most to the variance (PC1 and PC2) are shown in Fig. 2A. The parameters closest to the circle are most represented in the projection and their distances to PC1 and PC2 axes indicate whether they contribute most to PC1 or PC2. PC1 is mainly related to the aggregate size characterized by its median diameter $D(0.5)$, the density values and, to a lesser extent, to the specific surface area. PC2 is essentially related to the Hausner ratio, the agglomerate size $D(0.5)$ and the agglomeration ratio (size ratio agglomerate/aggregate).

The scores plot in Fig. 2B shows three distinct clusters of samples. Samples of Group A highlighted high density and large aggregate diameter as well as low A_{sp}. Most samples were in Group B characterized by relatively low agglomerate and aggregate diameters and by high Hausner

ratio. Finally, Group C was made of samples characterized by large agglomerate diameter and A_{sp} values. This distribution in clusters relies on a visual observation of the scores plot. This is open to some subjectivity.

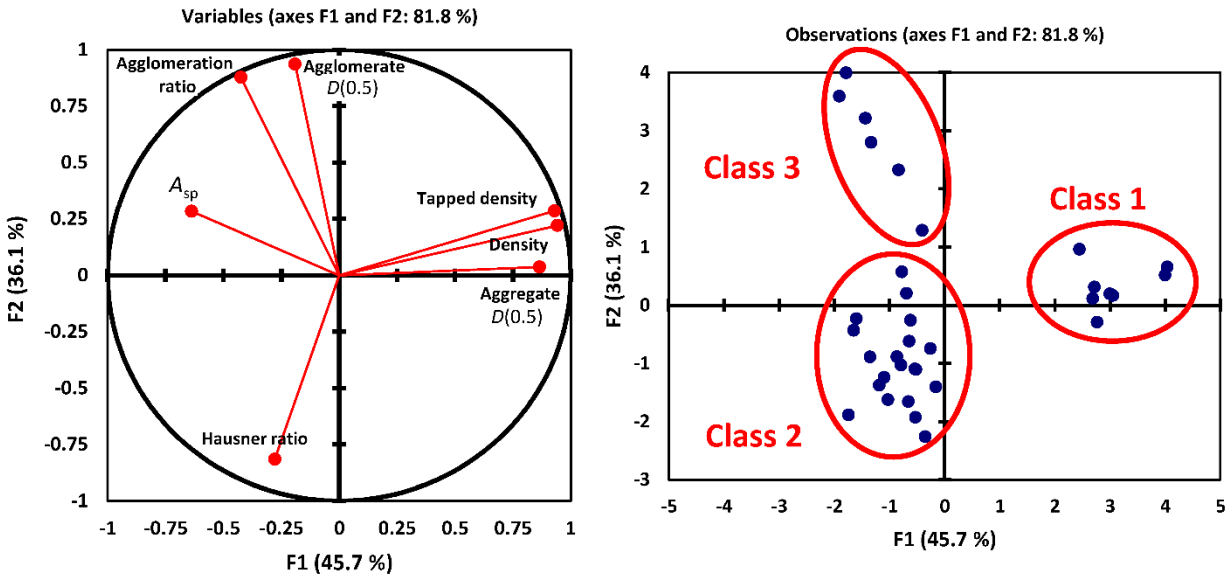

Figure 2. Loadings (A) and scores (B) plots obtained from the PCA analysis of the 34 ZnO samples characterized by 7 physicochemical parameters mapped onto the first two principal components PC1 and PC2 providing a cumulative variance of 81.8 %.

A more rigorous analysis of clustering relying on statistics makes use of Hierarchical Ascendant Clustering (HAC). The outcome of HAC is a tree called 'dendrogram' where the population of samples distributes into classes (clusters) according to the Euclidian distance between samples called dissimilarity (Fig. 3). The dissimilarity that minimizes the intra-cluster variance and maximizes inter-cluster variance according to Ward's criterion [12] was 53 (the dashed line in Fig. 3). The dendrogram from HAC calculations indeed indicates three clusters of samples as it has been inferred by visual observation of PCA results in the PC1–PC2 frame. So HAC analysis yielded three clusters according to a statistical analysis that made the clustering process free of subjectivity.

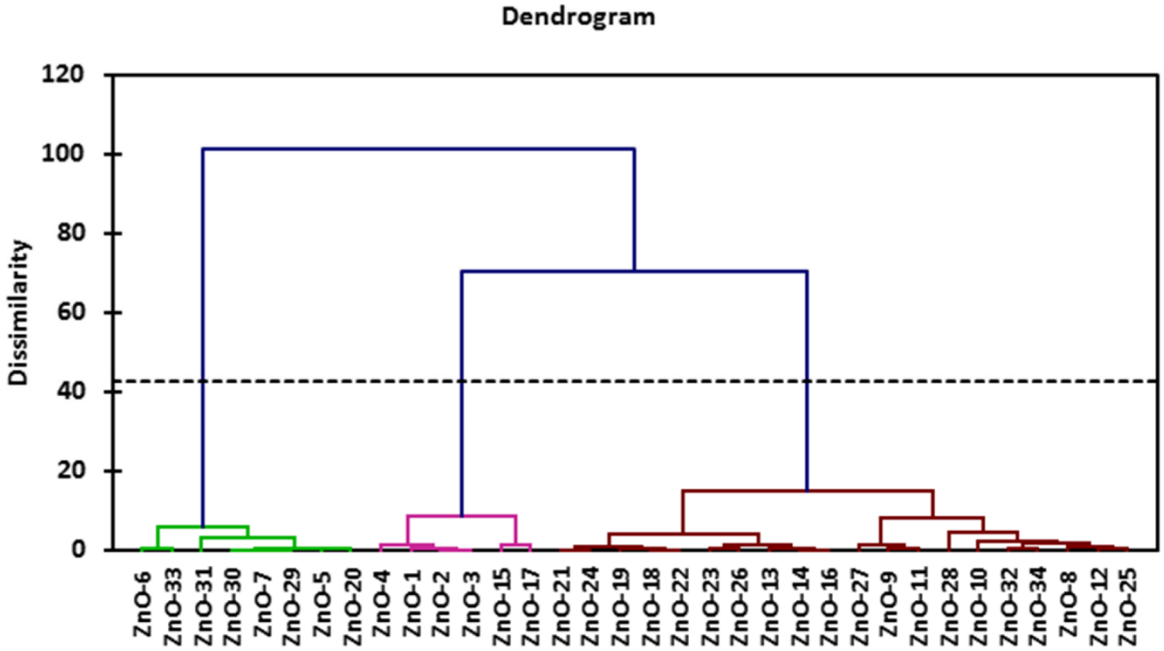

Figure 3. Hierarchical Ascendant Clustering Dendrogram obtained from the analysis of the 34 ZnO samples described by the 7 standardized physicochemical parameters. The dashed line shows the optimum dissimilarity inferred from the Ward's criterion.

Class 1 are samples mainly characterized by high density, low A_{sp} and large aggregate median diameter. These samples exhibited density larger than 2 g·cm^{-3} while samples belonging to other clusters of the dataset had density lower than 1.2 g·cm^{-3} (Fig. 4A). Except for the ZnO-31 sample with 6.6 µm aggregate diameter, samples of Class 1 were made of the largest aggregates with $D(0.5)$ ranging from 12.9 to 27.6 µm (Fig. 4B). Aggregate sizes measured by light scattering corresponded to the size of primary particles estimated from electron microscopy (Fig. 1A). Those samples are not aggregated and they are slightly agglomerated. Indeed, the mean value of agglomeration ratio took the low value of 2.2 (Fig. 4C). This mean shifted down to 1.7 if the ZnO-31 sample was discarded. Values close to one mean that particles are not agglomerated. In accordance to their large particle size and high density, Class 1 samples had small specific surface areas that corresponded to the smallest values observed in the dataset (A_{sp} < 0.5 m^2·g^{-1}) (Fig. 4D).

The 22 samples of Class 2 exhibited low density and presence of both small aggregates and agglomerates. The agglomeration ratio was widely scattered, which meant that some samples of Class 2 were agglomerated whereas some others were not. Finally, Class 3 includes six samples made of small aggregates and large agglomerates ($D(0.5)$ > 100 µm) leading to the highest values of the agglomeration ratio (> 20, Fig. 4C). They also exhibit the highest specific surface areas (A_{sp} > 25 $m^2 \cdot g^{-1}$, Fig. 4D).

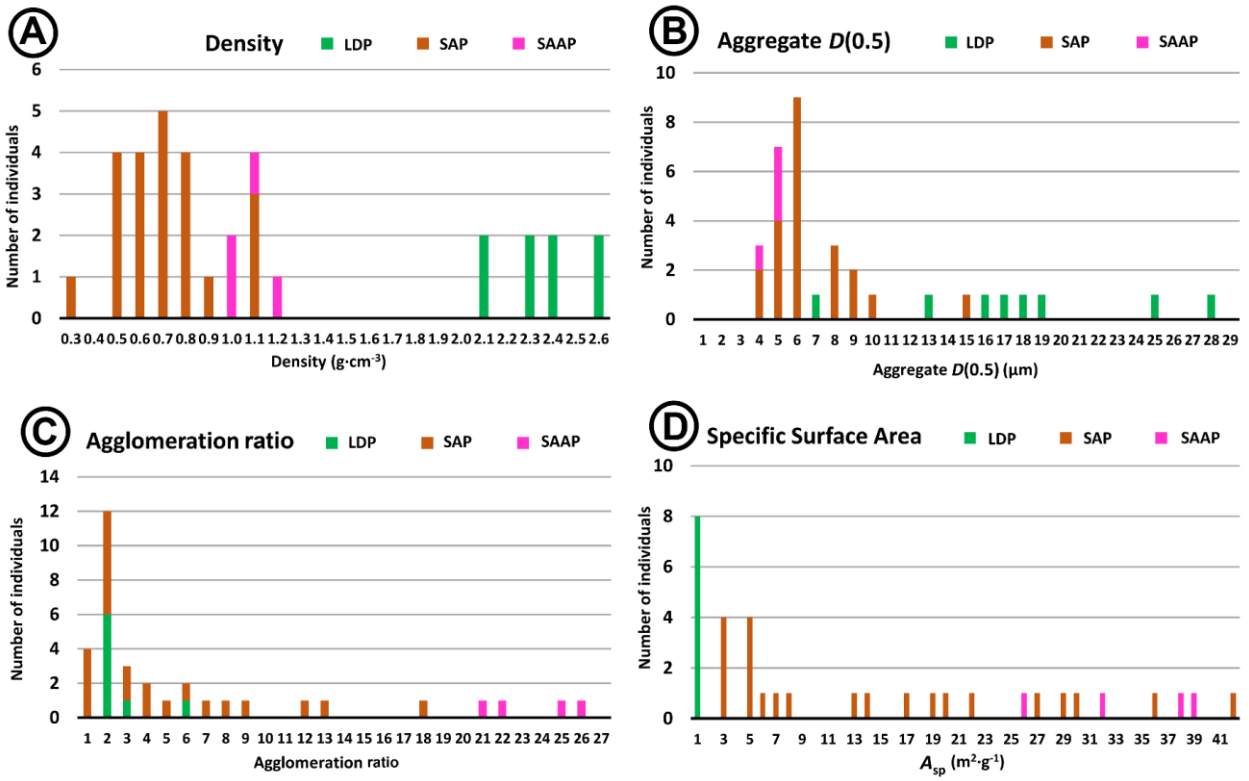

Figure 4. Distribution of physicochemical parameters. (A) density, (B) aggregate $D(0.5)$, (C) agglomeration ratio, (D) specific surface area.

As a summary of the clustering analysis, three different groups of samples were highlighted and they were described by their characteristic physicochemical properties. Names have been allocated to the groups according to their main physicochemical features:

- ‘Large dense particles’ (LDP): Class 1 is made of large massive particles that are not agglomerated. The high density and electron microscopy pictures show that such particles are dense (massive) and not aggregated. The specific surface area is low because the particles are large and dense (not porous). Adsorption and desorption of nitrogen do not show hysteresis in BET measurements. This class probably corresponds to zinc oxide manufactured by the ‘American process’ [14] and subsequently grinded.

- ‘Small aggregated and agglomerated particles’ (SAAP): Class 3 is made of very small elementary particles as disclosed by electron microscopy observations. As a consequence, density and tapped density of dry powders are low. Such ZnO grades were probably produced by the ‘French process’ or the ‘wet process’ (precipitation from a solution) [14]. Extensive agglomeration may come from a drying process by spray drying.

- ‘Small aggregated particles’ (SAP): Class 2 samples are also made of very small elementary particles. They are aggregated and only part of them is agglomerated. The dry densities are low (less than 1 $g \cdot cm^{-3}$). But their characteristics are spread over the wide range for the other physicochemical parameters. The SAP class is a grey area where aggregates are either not or weakly agglomerated (less than for the SAAP class). Their manufacture process is the same type as for the SAAP class.

3.3. Dissolution kinetics

Solubility and rate of dissolution are important parameters that characterize powder particles [18,19]. When assessing the solubility of feed compounds, dissolution rate gives a clear impression of the digestion process rather than solubility. The dissolution kinetics illustrates how fast a given element solubilizes, and this might have an impact on feed interactions, absorption and passage

rate of that element. Solubility is a state of equilibrium of a medium, but when the topic is digestion, solubility does not correctly address the questions, as reaching equilibrium of solubility can take longer time than digestion itself. Dissolution kinetics, though, will show how fast or slow a given feed compound takes to achieve equilibrium solubility.

Avramescu *et al.* [19] summarized studies using different conditions to mimic biological fluids such as medium pH and temperature according to the purpose of each study. The authors report the difficulties to assess kinetics in these media due to their complexity. Nevertheless, pH and temperature are key parameters influencing dissolution of metals in *in vitro* assays, and biological medium may have constituents, such as organic and inorganic ligands that may increase or decrease dissolution, and therefore impact understanding the dissolution mechanism of compounds [19,20]. Owing to such issues, the authors suggest a first screening to evaluate dissolution kinetics, in water medium, at a specified pH and temperature according to the purpose of the study.

In this study, the dissolution kinetics was assessed in water at pH 4 at 40 °C. Temperature and pH were selected to simulate the gastric pH of monogastric animals. Water medium was selected as to minimize the interactions with medium components and therefore have a better understanding of powders behavior.

ZnO does not dissolve in water as ZnO species but mainly as Zn^{2+} ions. There are actually several soluble zinc species, Zn^{2+}, $ZnOH^{+}$, $Zn(OH)_2$, $Zn(OH)_3^{-}$, and $Zn(OH)_4^{2-}$, that the respective concentrations depend on the pH. This is well-documented since Reichle *et al*. **[7]**. Zn^{2+} is the predominant species at pH 4; it is 99.99% of the full soluble zinc. Only Zn^{2+} ions are considered in the following. Dissolution of ZnO is a hydrolysis of ZnO into Zn^{2+} according to the chemical reaction

$$ZnO + H_2O \rightarrow Zn^{2+} + 2\ OH^{-} \quad (4)$$

Such reaction releases hydroxide ions (OH^-), so that, the pH increases when ZnO is dissolving into water. Maintaining the pH constant during the dissolution process requires addition of acid. Such demand for acid corresponds to the amount of OH^- ions released according to the dissolution reaction, Eq. (4). As two moles of OH^- ions are released for each mole of dissolved ZnO, the number of H^+ moles to be supplied is twice the number of moles of dissolved Zn^{2+}. In that way, the volume of acid supplied as a function of time can be converted into the concentration of dissolved Zn^{2+}, that is, into dissolution kinetics of ZnO. An automatic burette was used to deliver hydrochloric acid (HCl 1 M) in such a way that the pH is regulated at a constant value; the volume of added acid was recorded as a function of time.

$$[Zn^{2+}] = \frac{\text{Volume of acid supplied} \times [HCl]}{2 \times \text{Volume of solution}} \quad (5)$$

This method designed for easy measurement of dissolution kinetics is indirect and relies on the assumption of the chemical reaction, Eq. (4), being unique. This assumption was validated by comparison to direct measurements of soluble Zn by ICP-OES in samples collected during dissolution experiments. ICP-OES provides the concentration of soluble zinc, whatever its speciation (chemical form). The concentrations of soluble Zn determined by this method were in very good agreement with those determined by ICP-OES (Fig. 5); so, the method using the automatic burette was satisfactorily validated.

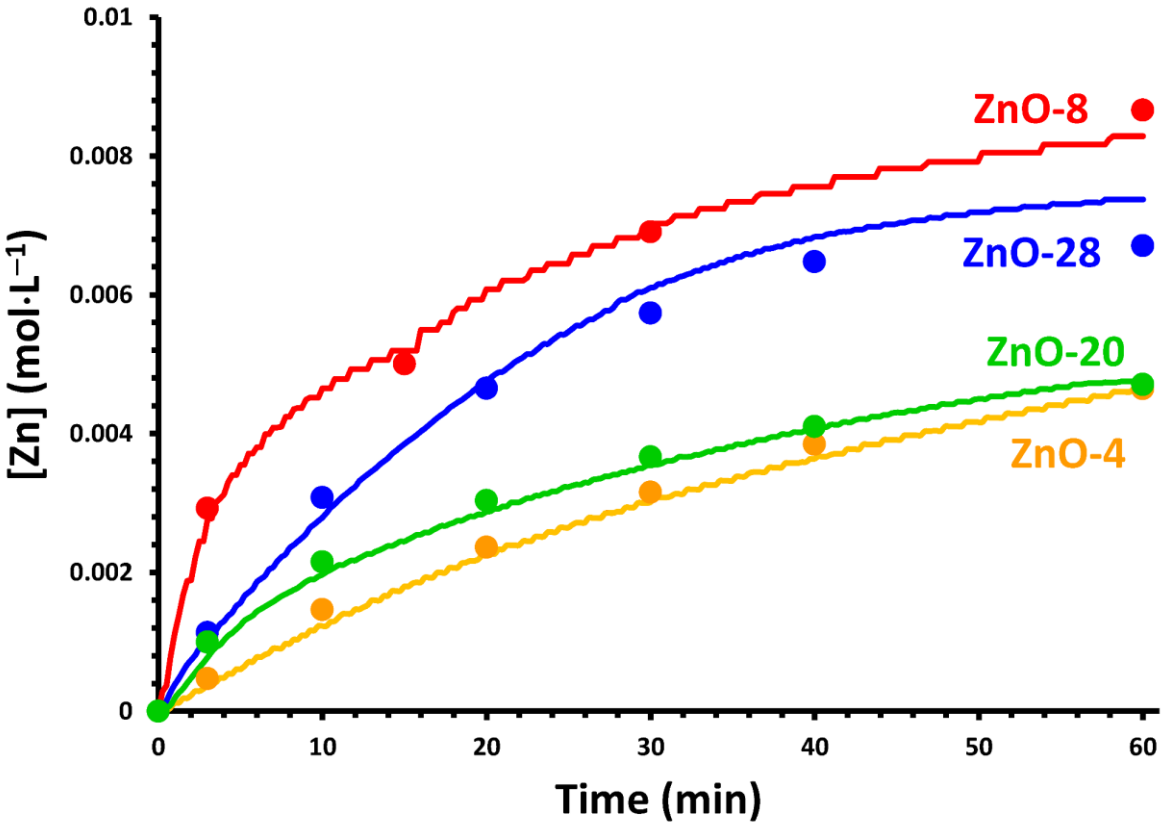

Figure 5. Dissolution kinetics of ZnO in water at pH 4 at 40 °C. The continuous line stands for kinetics measured using the burette and data points pertain to ICP-EOS measurements of Zn concentration in collected aliquots.

The dissolution kinetics was quite variable depending on the type of ZnO powder. ZnO powders dissolving the fastest reached full dissolution in less than 20 min, while the slowest samples did not reach 50% of dissolution during 1 h of experiment. The kinetics was characterized by the concentrations of Zn dissolved after 10 min and after 20 min for their use in statistical analyses. The purpose of this section is to search for correlations between dissolution kinetics and physicochemical properties. Samples from LDP and SAAP classes exhibited the slowest dissolution kinetics. The behavior of samples belonging to the LDP class may be obviously related to their low specific surface area. It is tentatively related to their highly agglomerated state for SAAP class since large size of agglomerates is a specific feature of SAAP class compared to SAP

class. Such visual observation of the influence of HAC clusters on dissolution kinetics clearly teaches that physicochemical properties control dissolution rate and that the clustering made by HAC can provide clues for understanding relationships between dissolution kinetics and physicochemical properties.

A correlation analysis was performed to further investigate such relationships. The Pearson's correlation coefficients (*R*) were determined from the whole dataset. The correlation matrix (Table 2) shows that the dissolution rate was significantly anti-correlated with the density parameters and with both the agglomerate and aggregate median diameters. As expected, this indicates that large aggregates or agglomerates and/or dense ZnO particles make the dissolution process slow. The correlation is stronger with the density than with aggregate or agglomerate size. This appears quite surprising because no significant correlation was obtained with A_{sp} since so many literature reports claim that dissolution is related to the available contact area of the solid and liquid media.

Table 2. Correlation matrix of Pearson's correlation coefficients, *R*, determined for the 34 ZnO samples. The significant *R* values (at 0.05 level of significance) are indicated in bold.

	Aggregate *D*(0.5) (µm)	**Agglomerate *D*(0.5) (µm)**	**Agglomeration ratio**	**Density (g·cm^{-3})**	**Tapped density (g·cm^{-3})**	**Hausner ratio**	**A_{sp} (m^2·g^{-1})**	**[Zn^{2+}] after 10 min (mol·L^{-1})**	**[Zn^{2+}] after 20 min (mol·L^{-1})**
Aggregate *D*(0.5) (µm)	1								
Agglomerate *D*(0.5) (µm)	-0.073	1							
Agglomeration ratio	-0.333	**0.945**	1						
Density (g·cm^{-3})	**0.764**	0.066	-0.150	1					
Tapped density (g·cm^{-3})	**0.783**	0.014	-0.204	**0.996**	1				
Hausner ratio	-0.172	-0.600	**-0.523**	**-0.460**	**-0.385**	1			
A_{sp} (m^2·g^{-1})	**-0.401**	0.309	**0.437**	**-0.422**	**-0.440**	0.012	1		
[Zn^{2+}] after 10 min (mol·L^{-1})	**-0.632**	**-0.479**	**-0.375**	**-0.709**	**-0.676**	**0.653**	0.171	1	
[Zn^{2+}] after 20 min (mol·L^{-1})	**-0.417**	**-0.419**	-0.304	**-0.777**	**0.749**	**0.621**	0.189	**0.982**	1

To illustrate these results, the zinc concentration after 10 min dissolution time was represented as a function of i) the density, ii) the agglomeration ratio, and iii) A_{sp} (respectively in Fig. 6A, B and C). The samples of LDP class appeared to strongly impact the correlation coefficients: they clearly induce a strong correlation with density (Fig. 6A) while they make it weaker with the size ratio (Fig. 6B). No significant linear relationship was observed between A_{sp} and the dissolution rate by considering the whole dataset (Fig. 6C). But these two parameters are quite related since all of the samples of LDP class characterized by the lowest A_{sp} values (≤ 0.5 $m^2 \cdot g^{-1}$) had low dissolution rates. The other samples (SAP and SAAP classes) with A_{sp} ranging from 2.0 to 41.0 $m^2 \cdot g^{-1}$ may exhibit all types of dissolution kinetics.

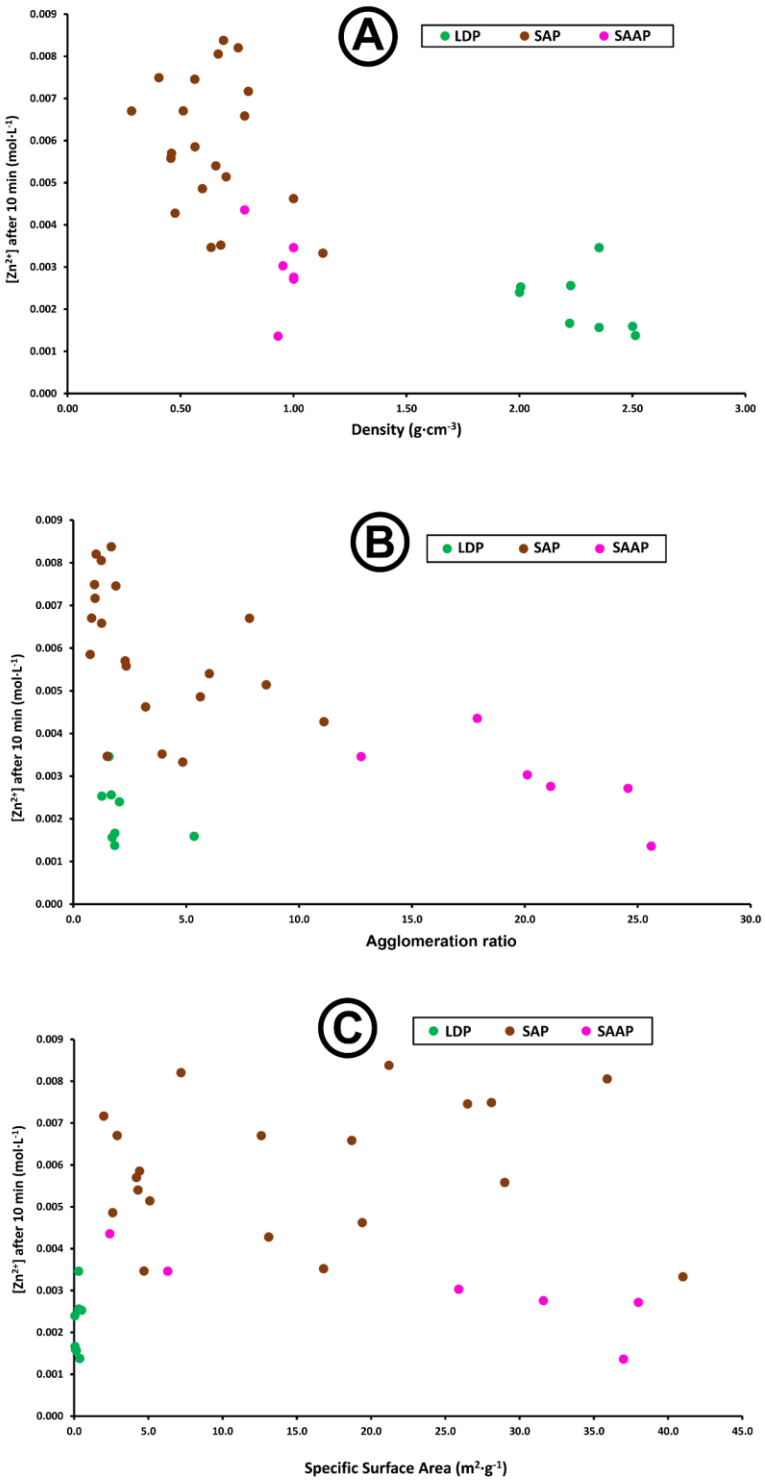

Figure 6. Zinc concentration after 10 min dissolution time as a function of density (A), agglomeration ratio (B) and A_{sp} (C) for the 34 ZnO samples.

A refined analysis was done by considering together samples of both SAP and SAAP classes. The corresponding correlation matrix (Table 3) disclosed that dissolution kinetics was significantly related to the agglomerate size, the agglomeration ratio, and the dry density parameters. For both dissolution measurements, the highest *R* values were obtained for the agglomeration ratio. The negative correlation coefficient indicated that dissolution was favored in ZnO samples characterized by low size ratios, i.e. by aggregates that were poorly agglomerated. As in the correlation analysis of the full dataset, the dissolution was improved for samples exhibiting low density revealing large porosity of the aggregates. The striking feature is that dissolution kinetics is not correlated with A_{sp}.

Table 3. Correlation matrix of Pearson's correlation coefficients determined for the 26 samples of merged SAP and SAAP classes. The significant *R* values (at 0.05 level of significance) are indicated in bold.

	Aggregate *D*(0.5) (µm)	**Agglomerate *D*(0.5) (µm)**	**Agglomeration ratio**	**Density ($g \cdot cm^{-3}$)**	**Tapped density ($g \cdot cm^{-3}$)**	**Hausner ratio**	**A_{sp} ($m^2 \cdot g^{-1}$)**	**$[Zn^{2+}]$ after 10 min ($mol \cdot L^{-1}$)**	**$[Zn^{2+}]$ after 20 min ($mol \cdot L^{-1}$)**
Aggregate *D*(0.5) (µm)	1								
Agglomerate *D*(0.5) (µm)	-0.080	1							
Agglomeration ratio	-0.206	**0.972**	1						
Density ($g \cdot cm^{-3}$)	-0.012	**0.551**	**0.513**	1					
Tapped density ($g \cdot cm^{-3}$)	0.086	0.377	0.325	**0.957**	1				
Hausner ratio	0.264	**-0.683**	**-0.702**	**-0.483**	-0.215	1			
A_{sp} ($m^2 \cdot g^{-1}$)	0.094	0.309	0.345	0.376	0.312	-0.221	1		
$[Zn^{2+}]$ after 10 min ($mol \cdot L^{-1}$)	0.347	**-0.700**	**-0.751**	**-0.558**	**-0.401**	**0.617**	-0.236	1	
$[Zn^{2+}]$ after 20 min ($mol \cdot L^{-1}$)	0.302	**-0.701**	**-0.753**	**-0.587**	**-0.440**	**0.594**	0.295	**0.982**	1

It remains the LDP class where the small number of individuals compromises the accuracy of its statistical analyses. It is characterized by a low A_{sp}; but A_{sp} does not significantly contribute to the variance of the whole dataset (Fig. 6C). Fig. 6C shows the origin of such lack of correlation between dissolution rate and A_{sp}: samples with low dissolution rate are those with the lowest A_{sp} (LDP class) and the highest A_{sp} (SAAP class). All samples of the LDP class have a low A_{sp} and a

slow dissolution rate, so that a low A_{sp} is indeed associated to a slow dissolution. Fig. 6C shows two different regimes of dissolution according to the A_{sp}. Dissolution rate increases with respect of A_{sp} for samples with A_{sp} lower than 2 $m^2 \cdot g^{-1}$, and stays more or less constant for higher A_{sp} with a large scatter of data points that prevents a statistical correlation. So, it can be inferred that the A_{sp} parameter controls dissolution for samples with low A_{sp}, even though this is not an outcome of the correlation analysis.

3.4. Dissolution mechanism

The dissolution rate is often claimed directly proportional to A_{sp} of the powder, meaning that the smaller the particles, the faster dissolution happens [21]. This view is contradicted in many instances however, and agglomeration has been put forward as a rationale to slow dissolution [22,23,24]. Dissolution kinetics showed a negative correlation with A_{sp} in the current experiments. Statistical analysis revealed a greater influence of agglomerates to dissolution. Agglomeration appears in the parameters of higher statistical relevance: agglomerate size, agglomeration ratio, density and tapped density. The rate-limiting step in the kinetics of dissolution is controlled by the structural arrangement of particles.

A first step for dissolution is contacting water and solid particles. The surface properties of ZnO are quite complicated because this material has polar and nonpolar crystallographic planes [25]. However, total wetting of ZnO surface by water was ensured in the present cases. Indeed, the ZnO powders got finely dispersed in the bulk of water immediately as the powders were dusted into water. This simple observation is equivalent to an immersion wettability experiment [26]. Wettability of ZnO was not a limitation to dissolution; it is ignored in the following. However, ZnO aggregates of primary particles did not break upon dispersion in water. Peptization of

aggregates/agglomerates is indeed an efficient mean to speed up dissolution; it would require operating agglomeration with the help of binders that can act as dispersing agents [27,28,29]. This is not the present case. The mechanism by which ZnO is dissolving into a stirred medium is split in a two-step process: (1) the dissolution itself at the surface of particles, and (2) the diffusion of soluble species to the bulk liquid medium. The dissolution kinetics is determined by the rate of the slowest step. Dissolution at the surface of solid particles is the same for all samples because all of them have the same zincite crystalline structure. There is no way it can change because ZnO has only one known crystalline phase. The geometry of the medium where diffusion takes place is of primary importance. For dense solid particles (non-porous), diffusion occurs in the quiescent layer of liquid contacting the solid surface. Its thickness is set by the efficiency of stirring and its area is that of the solid. Diffusion to bulk occurs in any case, even in a stirred medium where diffusion occurs in the stagnant layer. Dissolution happens faster in powders with high specific area. This is the classical 'naive' picture of dissolution process that presently holds for the LDP class. When diffusion is fast because efficient stirring leaves a thin stagnant layer, reaction-limited dissolution may occur. Diffusion inside aggregates/agglomerates is the rate-limiting step for the SAP and SAAP classes as it has been inferred by David *et al*. [18] who studied ZnO samples belonging to SAP and/or SAAP classes. Diffusion out of agglomerates is slow and it does not depend on the surface area of the solid. The way soluble species can escape outside the agglomerates may be quite long when agglomerates are of a large size (Fig. 7), so that dissolution is slow. As to stick to the classical picture of diffusion through a quiescent layer, the thickness of the later is no longer set by the stirring efficiency, but by the size of the agglomerates. The relationship between density, agglomerate size and dissolution comes from their relationship with the length of the path from the solid–liquid interface to the bulk medium, that is, the diffusion distance for escaping the

agglomerate. Large agglomerates as in the SEM picture of Fig. 1D are quite efficient at slowing down dissolution.

Aggregation can be taken as a parameter for controlling dissolution kinetics when the reaction-limited dissolution is slowed again by diffusion inside aggregates. This same idea is widely developed in the pharmaceutical field for dissolution control of tablet dosage forms. It might be thought at first sight that dissolution rate is controlled by porosity of the tablet material. This is actually not the case in instances where the rate-limiting step is dissolution of primary particles [30].

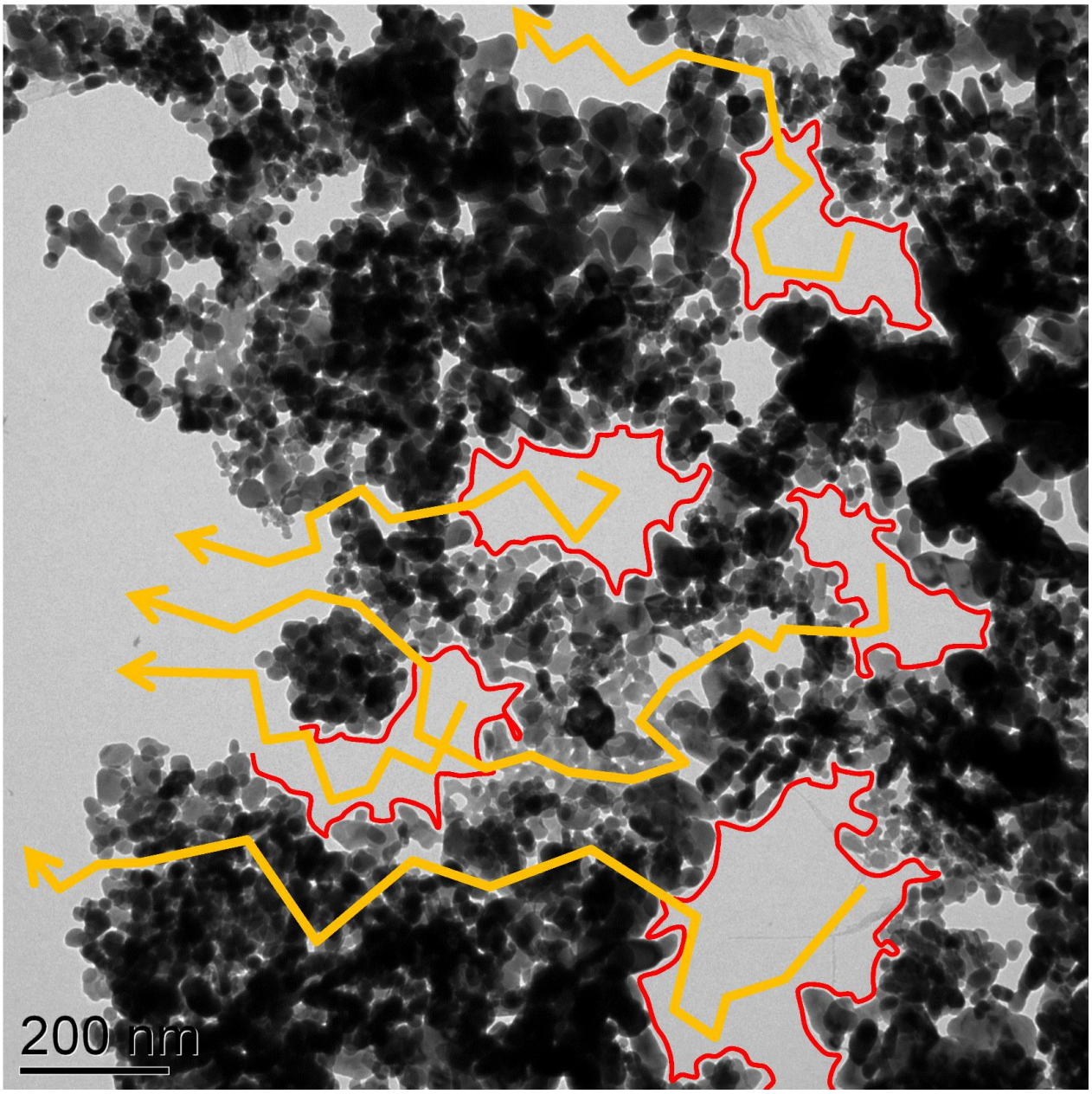

Figure 7. Illustration of proposed the two-step dissolution mechanism of ZnO of the SAP and SAAP classes. The first step is dissolution of ZnO at the surface of the solid (at red lines), followed by a second step of diffusion of soluble species through the confined quiescent medium to the stirred bulk solution (orange arrows).

3.5. Modeling dissolution kinetics

The first step prior to modeling is the selection of a physicochemical mechanism of dissolution that leads to the choice of the model [31]. Among the various dissolution models mainly developed

in the framework of extractive hydrometallurgy [32] as “Shrinking Particle”, “Shrinking Core – Constant Particle Size”, and mixed “Shrinking Core – Shrinking Particle” [31], the model of shrinking particles is presently the correct one as the full solid goes into solution. A clear solution is obtained at the end of dissolution and there is no residual ash.

Equations (1) and (3) expressing the flux at the surface of particles for the diffusion-limited, reaction-limited dissolution and mixed reaction–diffusion models have the same mathematical form. They write as a differential equation with the concentration $C(t)$ as a variable as

$$\frac{\mathrm{d}C(t)}{\mathrm{d}t} = k\,A(t)\,[C_S - C(t)] \qquad (6)$$

k is a phenomenological constant related to the diffusion or the dissolution reaction, depending on the process is diffusion-limited or reaction-limited. Eq. (6) can be integrated in order to yield kinetics profiles that can be directly compared to experiments. Such integration has already been done under restrictive conditions of constant area and/or constant bulk concentration. Thus, integration of the Noyes–Whitney or Nernst–Brunner equation in condition of constant area yields the kinetics profile as an exponential increase of bulk concentration [33,34,35,36]. Significant deviations from the exponential behavior has been observed for the dissolution of ZnO in environmental conditions [37]. Integration of Eq. (3) of reaction-limited dissolution has been done in the two particular cases of constant area (constant size) [18] and constant bulk concentration corresponding to ‘sink’ conditions [38]. In the present case, neither surface area nor bulk concentration is constant.

Integration of Eq. (1) for diffusion-limited dissolution has been given by Hixson and Crowell [39] in the case of shrinking particles where the size of solid particles decreases during the course of dissolution. For isotropic dissolution, the surface area varies as the power 2/3 of the decreasing solid volume. So, the area decreases as $A(t) = k_A[C_0 - C(t)]^{2/3}$ in the course of the dissolution

process according to the amount of ZnO present in particles, that is, the concentration remaining to be dissolved. C_0 is the final concentration reached at full dissolution; it is known from the full amount of ZnO and volume of liquid medium. k_A is proportional to the specific surface area of the solid powder. Substituting into Eq. (6) yields

$$\frac{dC(t)}{dt} = K[C_0 - C(t)]^{2/3}\,[C_S - C(t)] \qquad (7)$$

K is a composite constant that combines the constant k of Eq. (6) and k_A. The final result is an analytical relationship expressing the time as a function of bulk concentration [39]

$$t = \frac{1}{Ka^2}\left\{\sqrt{3}\,\tan^{-1}\left[\frac{2\sqrt{3}\,a(b-x)}{3a^2+(2b-a)(2x-a)}\right] + \frac{1}{2}\ln\left[\frac{(a+b)^2(a^2-ax+x^2)}{(a+x)^2(a^2-ab+b^2)}\right]\right\} \qquad (8)$$

with $a = (C_S - C_0)^{1/3}$, $b = {C_0}^{1/3}$, and $x = (C_0 - C)^{1/3}$.

Eq. (8) is the exact result of mathematical integration; it is preferred to more simple equations [32] that are often used because they allow more direct comparison with experimental data. However, they have been derived under mathematical approximations that the validity should be checked against. The experimental kinetic profile can be compared to Eq. (8). Alternatively, the derivative of the experimental data, dC/dt, can be compared to Eq. (7). Fitting Eq. (8) to the experimental data may be preferred because calculation of the derivative of experimental data introduces noise. However, Eq. (8) has a complex mathematical form where it is difficult to infer the influence of the parameters K and C_S. A comparison of the experimental dC/dt to Eq. (7) helps at devising the validity of the theoretical equations. The model was fitted to the experimental data by minimizing the objective function, F, for N data points and p adjustable parameters K, C_S and C_0 (p = 3) as the sum of square deviations weighted by the concentration intervals corresponding to each of the data points of the digital experimental record

$$F = \frac{1}{(N-p)}\sum_{i=1}^{N}\Delta C_i\left(t_{i,\mathrm{exptl}} - t_{i,\mathrm{calc}}\right)^2 \qquad (9)$$

The model systematically underestimated the zinc release at the end of dissolution. The faster experimental dissolution rate may be due to an increase of the chemical potential of zinc in the solid particles as they reach very small size according to Kelvin law [40]. The fit of the model was restricted to 80 % of the dissolution for avoiding this bias. Small nanoparticles may dissolve faster because the solubility of ZnO is higher for smaller nanoparticles according to Kelvin law. This effect is only significant for very small nanoparticles. Particles shrinkage during dissolution (accounted for in Eqs (7) and (8)) makes a much higher contribution. Indeed, the size dependence of dissolution kinetics of very small ZnO nanoparticles (down to 4 nm diameter) could not be rationalized on the basis of the sole Kelvin law [41].

Typical data of LDP, SAP and SAAP samples for which the theory fits well to experiments are shown in Fig. 8. However, there are samples for which the theory obviously does not match. This point will be addressed later in the text.

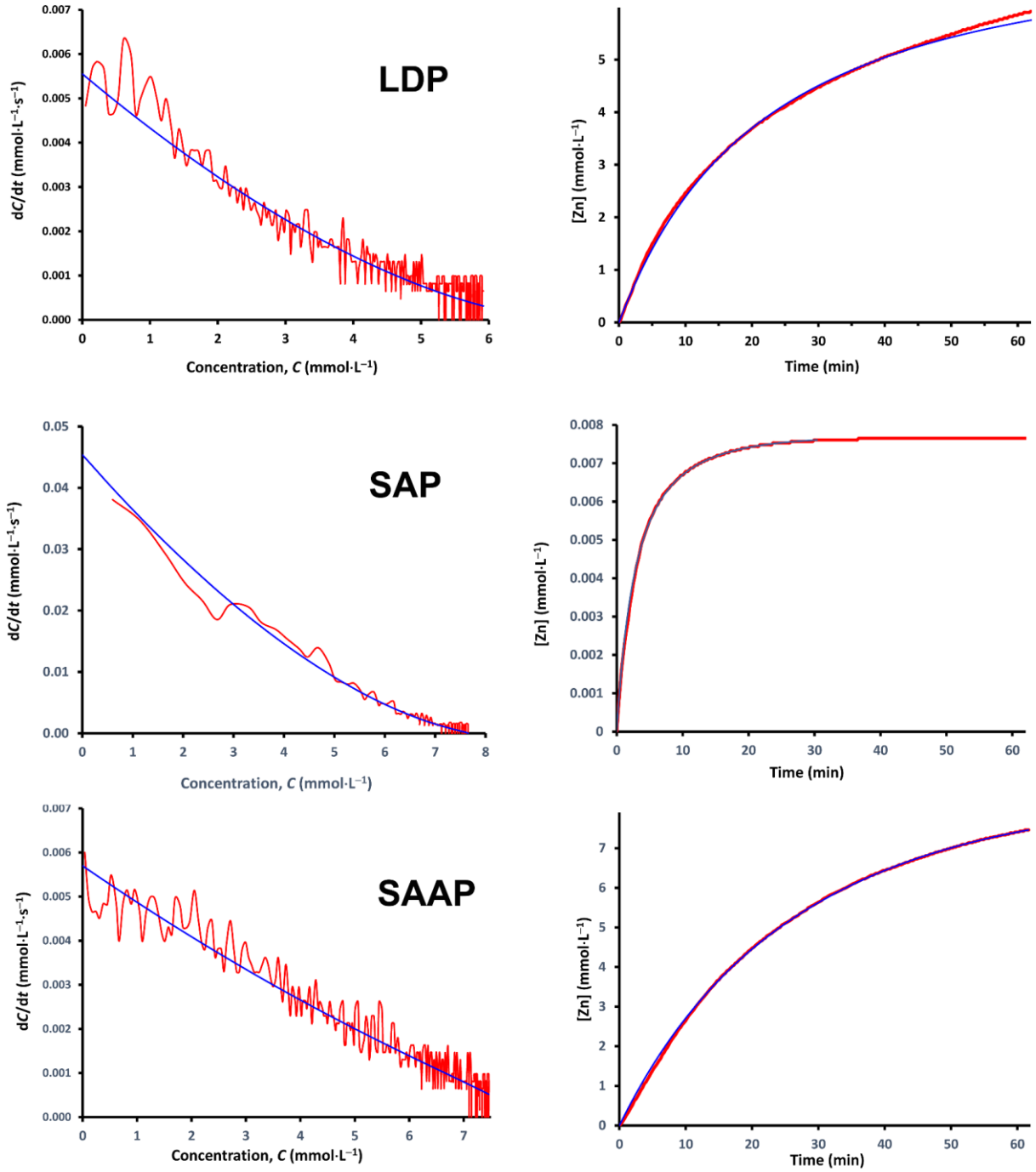

Figure 8. Direct check against the kinetic model using the time-derivative of experimental released concentration d*C*/d*t* against *C* (left side) and kinetic profile *C*(*t*) (right side) for samples taken from the three classes: LDP (ZnO-5), SAP (ZnO-22) and SAAP (ZnO-4). Red line is experimental and blue line is calculated from Eq. (7) or Eq. (8).

For samples of the LDP and SAP classes, the variation of dC/dt with respect to C clearly showed a curvature coming from the contribution of the term $[C_0 - C(t)]^{2/3}$. Conversely, samples belonging to the SAAP class showed a linear variation of dC/dt vs C, that might mean that the model of diffusion or reaction rate depending on surface area was not valid. The fit of the model was quite satisfactory however because of the mathematical properties of Eq. (7). Thus, curvature of dC/dt vs C is upwards when $C_S < 2\ C_0$, it is downwards when $C_S > 2\ C_0$, and there is no apparent curvature when C_S is close to $2\ C_0$. In the case of SAAP where the experimental variation of dC/dt vs C is linear, fitting Eq. (7) or Eq. (8) to experimental data by mathematical minimization of deviation between experiment and theory forces $C_S = 2\ C_0$. For LDP and SAP classes, the outcome of fitting was always $C_S < 2\ C_0$. So C_S was larger for samples of the SAAP class, which makes sense as diffusion was the slowest for this class. A slow diffusion of Zn^{2+} and OH^- to the bulk causes higher accumulation of soluble species in the liquid close to the solid surface. At the end the same model holds for all samples though the rate-limiting steps are different because the same mathematical form of the equations holds whatever the exact mechanism. The selection of a suitable model is the most critical step of modeling [31]. The present model is of quite general breadth. This is advantageous as it can describe the whole series of samples; but the drawback is that it does not help at discriminating different mechanisms.

Model fitting provided optimized values of C_0, C_S and K. The value of C_0 was adjusted because any difference between predicted and actual values would cause systematic deviations that bias the error minimization. Adjusted C_0 values were close to C_0 = 8–9 mmol·L^{-1} expected according to the amount of ZnO and volume of water in dissolution experiments. The value of ZnO solubility that came out of model fitting was low since $C_S < 2\ C_0$ whereas the solubility of ZnO at pH 4 is very high. The solubility of ZnO has never been measured in such acidic medium. It was estimated

by extrapolation of measurements performed in more basic media using equilibrium constants given by Reichle *et al.* [7] Let us notice that Reichle *et al.* reported the solubility product of zinc hydroxide $Zn(OH)_2$ whereas the present study deals with zinc oxide ZnO. There is actually no significant difference between solubility products of $Zn(OH)_2$ ($Log(K_{SP}) = -16.76$) [7] and previous determinations for ZnO that a compilation is given by Wesolowski *et al.* [42] (the mean value $Log(K_{s0}) = 11.2$ yields $Log(K_{SP}) = -16.8$). Data by Reichle *et al.* were preferred because they considered all soluble species of zinc whereas earlier measurements only considered the sole equilibrium between ZnO and Zn^{2+}. The solubility extrapolated at pH 4 assumed an unrealistically high value $C_S = 1740\ mol{\cdot}L^{-1}$; the actual solubility of ZnO in acidic medium should be that of the $ZnCl_2$ salt formed by reaction of ZnO with hydrochloric acid. It is again very high. The solubility of $ZnCl_2$ in water is 80 wt% at 25 °C [43]. In the present case, the solubility of zinc that matters is the local saturation concentration in the solution contacting the solid surface. Hydrolysis of ZnO releases Zn^{2+} and OH^- ions at the same time. When diffusion to the bulk is slow, accumulation of hydroxide ions makes the solution basic close to the surface and the solubility strongly shifts down. The mean value of local solubility that came out of the model was $10^{-2}\ mol{\cdot}L^{-1}$, which corresponded to a local pH of 6.25. The minimum solubility of zinc hydroxide at 40 °C is $5.5\ \mu mol{\cdot}L^{-1}$ at pH 10 [7]. As production of hydroxide ions at the surface depends on time because the surface area is decreasing, its local concentration may vary during the course of dissolution, unless a stationary regime sets up such that hydroxide release is exactly compensated by diffusion to the bulk. It cannot be expected that the local solubility is constant. It was assumed constant in the model. A refinement of the model would require going in more details into the surface chemistry of ZnO dissolution. The local solubility should be considered as a phenomenological parameter accounting for accumulation of hydroxide ions at the surface of ZnO.

Despite the imperfections of the model, the value of the constant K can be taken for a discussion of dissolution mechanisms. A plot of K against the specific area A_{sp} (Fig. 9A) is widely scattered and the samples belonging to the different classes are mixed. Of course the statistical analysis disclosed that there was no correlation between dissolution rate and A_{sp}. However, data can be split into three families where dissolution kinetics linearly varies against A_{sp}: (*i*) fast increase of dissolution rate with respect to A_{SP} that corresponds to reaction-limited process, (*ii*) medium increase of dissolution rate where diffusion-control becomes predominant, (*iii*) slow increase of dissolution rate that corresponds to diffusion-limited process. Conversely, definite clusters can be seen in a plot of K against the tapped density (Fig. 9B); and they correspond to the classes defined from the Hierarchical Ascendant Clustering. Indeed, density and tapped density were correlated with dissolution kinetics in the PCA. Clusters are not as well-defined as in the PCA because the parameters that account most for the variance are the Principal Components which are linear combinations of the physicochemical parameters. The ratio of the constant K to the specific area, K/A_{sp}, accounts for the rate of the surface reaction of dissolution and/or diffusion through the quiescent liquid layer around the solid particles. At first sight, K/A_{sp} should be the same for all samples as it depends either on diffusivity and stirring conditions in case of diffusion-control, or on surface reaction rate constants k_+ and k_- in case of a reaction-limited process. K/A_{sp} actually varied a lot as shown in Fig. 9C. All data points appear aligned on a master curve that a regression to a power law is $K/A_{sp} = 1.64 \times A_{sp}^{-0.87}$.

The strong variation of K/A_{sp} (Fig. 9C) clearly indicates that the rate-limiting phenomena assume very different mechanisms, depending on the physicochemical properties of ZnO. This conclusion has already been reached from the statistical analyses by PCA and Correlation analysis. Solubility of ZnO at pH 4 is very high. The low value of solubility predicted by the model means

that dissolution is slowed down by the chemical reaction of ZnO hydrolysis. So there is reaction-control in all instances. This does not explain the variability of K/A_{sp} values. For the cases of slowest dissolution, a supplementary rate-limitation operates, namely diffusion in the stagnant liquid trapped inside aggregates and agglomerates. Dissolution is not only diffusion-limited in this case as surface reaction also slows down dissolution; it is reaction-diffusion-limited. It is worth noticing that such conclusions were not reached from the sole modeling; they come from an analysis of samples of various physicochemical properties. The most suitable tools are therefore correlation analyses by PCA. That K/A_{sp} looks correlated with A_{sp} as shown in Fig. 9C does not mean that dissolution is controlled by the contact area of the solid with the liquid. Actually, powders with small sizes of primary particle have a large specific area and they are strongly aggregated. There is no sample of non-aggregated of small nano-sized particles in the present collection. Such sample may exist as stable suspensions of nanoparticles; but aggregation caused by drying them is generally irreversible. There are very few cases of spontaneous peptization into free primary particles of powders used in technical applications. Dissolution should not break aggregates for the dissolution kinetics remains controlled by diffusion in the quiescent liquid inside aggregates during the whole dissolution process. Fragmentation/peptization occurring at the end of dissolution does accelerate kinetics in many instances [44,45,46], which does not look being the present case.

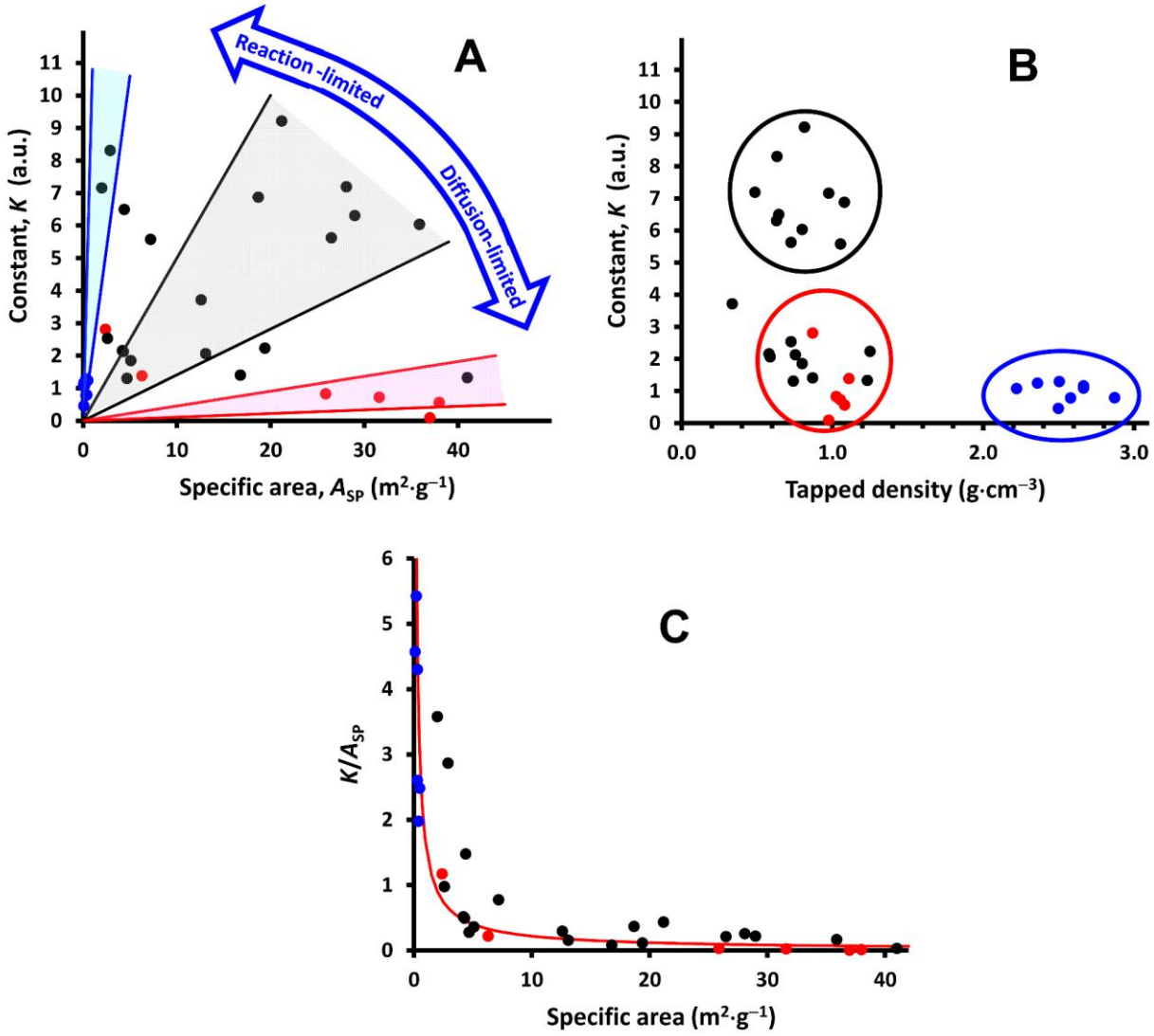

Figure 9. Analysis of the constant *K* of the dissolution kinetics model. Data points belonging to the different classes are given in colors: LDP in blue, SAP in black and SAAP in red. (A): *K* vs A_{sp} showing the transition to predominant limitation by reaction to control by diffusion. (B): *K* vs tapped density showing the clusters of data points. (C): K/A_{sp} vs A_{sp} together by the correlation line as a power law.

Finally, there were samples that the theoretical model did not fit. The main deviation from the model was a fast release of Zn^{2+} at short times. The origin of such misfit was a heterogeneous morphology of the ZnO particles, either the coexistence of small particles dissolving fast and coarse particles with slow dissolution kinetics (Fig. 10A), or the coexistence of particles with different shapes (needles and rounded) and surface area (Fig. 10B). Modeling the dissolution process would

require well-characterized samples with homogeneous characteristics. Samples of real life are not homogeneous. The way to manage with heterogeneous samples is applying statistical analyses in order to smooth off uncontrolled parameters and to avoid subjectivity in drawing conclusions. Otherwise the heterogeneity can be taken in consideration as a supplementary characteristic by implementation of a population balance model [47,48].

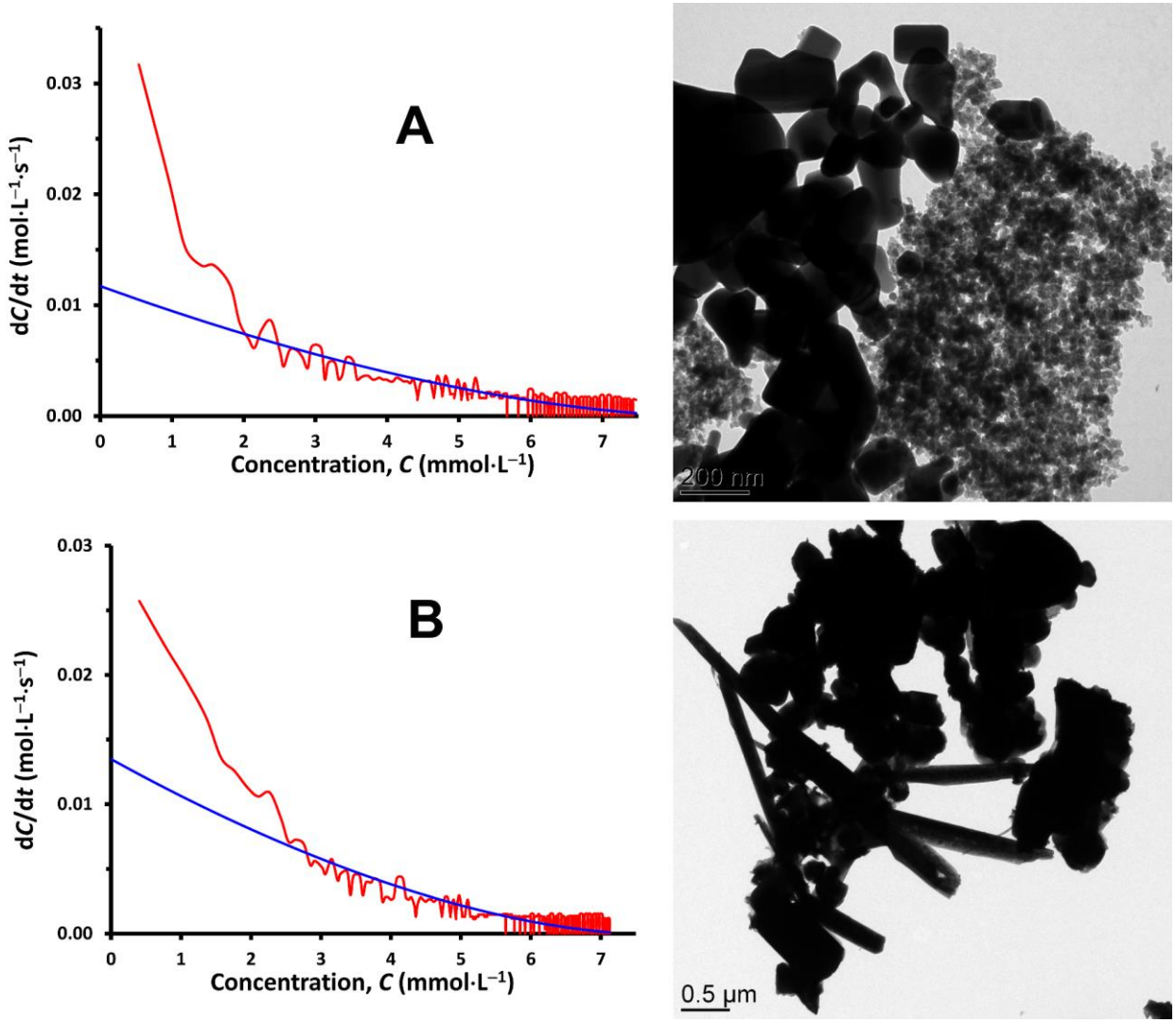

Figure 10. Kinetics of dissolution showing a fast dissolution at short time together with TEM pictures. (A) The fast dissolution component of ZnO-23 comes from few small particles mixed with the main large particles of a SAP sample. (B) ZnO-15 of the SAAP class contains needle-shaped particles together with rounded particles.

4. Conclusions

The present study disclosed large differences among evaluated sources of ZnO. Different physicochemical properties have an impact on the dissolution kinetics which can affect *in vivo* solubility and bioavailability in animals. Coarse and dense particles of low A_{sp} dissolve slowly as it is expected from common sense: small contact area with the liquid medium causes slow dissolution. The great majority of investigated feed grade ZnO powders are made of aggregates (and agglomerates) of small primary particles. A_{sp} is large; but dissolution can be slow. In this case, dissolution kinetics is limited by the slow diffusion through the quiescent liquid trapped inside aggregates related to the density of the powder. Bulk density is a way to assess aggregation and agglomeration of small primary nanoparticles. It is easy to measure and strongly correlated with dissolution rate. Slow dissolution can be achieved by using either coarse particles or large aggregates/agglomerates of small primary particles. The latter is preferred in practical applications because settling of suspensions is slower.

Studying the influence of the physicochemical parameters allows inferring the mechanism of dissolution, either diffusion-limited or reaction-limited. It is shown that decreasing the size of the primary particles causes aggregation and agglomeration that slows down diffusion of soluble species to the bulk liquid medium. So a transition from a reaction-limited to a diffusion-limited process occurs as the particle size goes smaller and aggregation operates.

With regards to the application to ZnO supplementation of animal feed, the control of dissolution kinetics is a tricky challenge. A fast dissolving ZnO source (called “highly soluble”) may overcome the uptake capacity of the gut, what would not happen in case of slow release from a coarse ZnO source [49]. Furthermore, fast solubilized minerals may interact with feed compounds [50]; an important one is phytate which is highly present in soya. Phytate binds Zn^{2+} ions in the

stomach (pH 2–4) and those complex species precipitate in the neutral medium of the duodenum (pH 6), compromising bioavailability [4]. Phytase enzymes are added to the diet in order to remedy this issue. The dissolution of ZnO should not be too fast, leaving a delay for phytase can eliminate free phytate in the stomach. ZnO should nevertheless dissolve for it is digested. There is a time window for dissolution requiring kinetic information as a selection criterion of a ZnO source.

Acknowledgements

DC is grateful to the Association Nationale de la Recherche et de la Technologie for a grant as a "bourse CIFRE" (n° 2016/0014) for the achievement of her PhD.

References

[1] J.-Y. Dourmad, C. Jondreville, Impact of nutrition on nitrogen, phosphorus, Cu and Zn in pig manure, and on emissions of ammonia and odours. Livestock Sci. 112 (2007) 192–198.

[2] P. Schlegel, Y. Nys, C. Jondreville, Zinc availability and digestive zinc solubility in piglets and broilers fed diets varying in their phytate contents, phytase activity and supplemented zinc source. Animal 4 (2010) 200–209.

[3] P. Schlegel, D. Sauvant, C. Jondreville, Bioavailability of zinc sources and their interaction with phytates in broilers and piglets. Animal 7 (2013) 47–59.

[4] D. Brugger, W. Windisch, Strategies and challenges to increase the precision in feeding zinc to monogastric livestock. Animal Nutr. 3 (2017) 103–108.

[5] A. Narcy, A. Roméo, N. Même, Y. Nys, S. Durosoy, Biodisponibilité de différentes sources d'oxyde de zinc chez le poulet de chair. 11èmes Journées de la Recherche Avicole et Palmipèdes à Foie Gras; Tours, France, 2015.

[6] M.N. Anwar, V. Ravindran, P.C.H. Morel, G. Ravindran, A.J. Cowieson, Effect of limestone particle size and calcium to non-phytate phosphorus ratio on true ileal calcium digestibility of limestone for broiler chickens. Br. Poult. Sci. 57 (2016) 707–713.

[7] R.A. Reichle, K.G. McCurdy, L.G. Hepler, Zinc hydroxide: solubility product and hydroxy-complex stability constants from 12.5-75 C. Can. J. Chem. 53 (1975) 3841–3845.

[8] H.M. Edwards, D.H. Baker, Bioavailability of zinc in several sources of zinc oxide, zinc sulfate, and zinc metal. J. Animal Sci. 77 (1999) 2730–2735.

[9] A. Berthoud, Théorie de la formation des faces d'un cristal. J. Chim. Phys. 10 (1912) 624–635.
[10] K.R. Gabriel, The biplot graphic display of matrices with application to Principal Component Analysis. Biometrika 58 (1971) 453–467.
[11] R.G. Brereton, Applied Chemometrics for Scientists. Wiley, Chichester, 2007.
[12] J.H. Ward Jr, Hierarchical grouping to optimize an objective function. J. Am. Stat. Assoc. 58 (1963) 238–244.
[13] B.S. Everitt, S. Landau, M. Leese, D. Stahl, Cluster Analysis, 5th edition, Wiley, Chichester, 2011.
[14] A. Moezzi, A. McDonagh, M. Cortie, Zinc oxide particles: synthesis, properties and applications. Chem. Eng. J. 185 (2012) 1–22.
[15] G. Nichols, S. Byard, M.J. Bloxham, J. Botterill, N.J. Dawson, A. Dennis, V. Diart, N.C. North, J.D. Sherwood, A review of the terms agglomerate and aggregate with a recommendation for nomenclature used in powder and particle characterization. J. Pharm. Sci. 91 (2002) 2103–2109.
[16] P. Borm, F.C. Klaessig, T.D. Landry, B. Moudgil, J. Pauluhn, K. Thomas, R. Trottier, S. Wood, Research strategies for safety evaluation of nanomaterials, Part V: Role of dissolution in biological fate and effects of nanoscale particles. Toxicol. Sci. 90 (2006) 23–32.
[17] A. Balakrishnan, P. Pizette, C.L. Martin, S.V. Joshi, B.P. Saha, Effect of particle size in aggregated and agglomerated ceramic powders. Acta Mater. 58 (2010) 802–812.
[18] C.A. David, J. Galceran, C. Rey-Castro, J. Puy, E. Companys, J. Salvador, J. Monné, R. Wallace, A. Vakourov, Dissolution kinetics and solubility of ZnO nanoparticles followed by AGNES. J. Phys. Chem. C 116 (2012) 11758–11767.
[19] M.L. Avramescu, P.E. Rasmussen, M. Chénier, H.D. Gardner, Influence of pH, particle size and crystal form on dissolution behaviour of engineered nanomaterials. Environ. Sci. Pollut. Res. 24 (2017) 1553–1564.
[20] C.A. David, J. Galceran, F. Quattrini, J. Puy, C. Rey-Castro, Dissolution and phosphate-induced transformation of ZnO nanoparticles in synthetic saliva probed by AGNES without previous solid−liquid separation. Comparison with UF-ICP-MS. Environ. Sci. Technol. 53 (2019) 3823–3831.
[21] M. Mosharraf, C. Nyström, The effect of particle size and shape on the surface specific dissolution rate of microsized practically insoluble drugs. Int. J. Pharm. 122 (1995) 35–47.
[22] B. Alway, R. Sangchantra, P.J. Stewart, Modelling the dissolution of diazepam in lactose interactive mixtures. Int. J. Pharm. 130 (1996) 213–224.
[23] P.J. Stewart, F.-Y. Zhao, Understanding agglomeration of indomethacin during the dissolution of micronised indomethacin mixtures through dissolution and de-agglomeration modeling approaches. Eur. J. Pharm. Biopharm. 59 (2005) 315–323.

[24] S. Muschert, F. Siepmann, B. Leclercq, B. Carlin, J. Siepmann, Drug release mechanisms from ethylcellulose: PVA-PEG graft copolymer-coated pellets. Eur. J. Pharm. Biopharm. 72 (2009) 130–137.
[25] C. Wöll, The chemistry and physics of zinc oxide surfaces. Prog. Surface Sci. 82 (2007) 55–120.
[26] M. Lazghab, K. Saleh, I. Pezron, P. Guigon, L. Komunjer, Wettability assessment of finely divided solids. Powder Technol. 157 (2005) 79–91.
[27] L. Forny, A. Marabi, S. Palzer, Wetting, disintegration and dissolution of agglomerated water soluble powders. Powder Technol. 206 (2011) 72–78.
[28] Y. Weerapol, S. Limmatvapirat, H. Takeuchi, P. Sriamornsak, Fabrication of spontaneous emulsifying powders for improved dissolution of poorly water-soluble drugs. Powder Technol. 271 (2015) 100–108.
[29] K. Pitt, R. Peña, J.D. Tew, K. Pal, R. Smith, Z.K. Nagy, J.D. Litster, Particle design via spherical agglomeration: A critical review of controlling parameters, rate processes and modeling. Powder Technol. 326 (2018) 327–343.
[30] M.A. Ansari, F. Stepanek, The effect of granule microstructure on dissolution rate. Powder Technol. 181 (2008) 104–114.
[31] O. Levenspiel, Chemical Reaction Engineering. 3rd edition, Wiley, New York, 1999, Chap 25, pp. 566–588.
[32] H.Y. Sohn, Fundamentals of the kinetics of heterogeneous reaction systems in extractive metallurgy. In: H.Y. Sohn, M.E. Wadsworth, (Eds.), Rate Processes of Extractive Metallurgy. Plenum Press, New York, 1979, Chap 1, pp. 1–51.
[33] A.A. Noyes, W.R. Whitney, Ueber die Auflösungsgeschwindigkeit von festen Stoffen in ihren eigenen Lösungen. Z. Phys. Chem. 23 (1897) 689–692.
[34] A.A. Noyes, W.R. Whitney, The rate of solution of solid substances in their own solutions. J. Am. Chem. Soc. 19 (1897) 930–934.
[35] W. Nernst, Theorie der Reaktionsgeschwindigkeit in heterogenen Systemen. Z. Phys. Chem. 47 (1904) 52–55.
[36] E. Brunner, Reaktionsgeschwindigkeit in heterogenen Systemen. Z. Phys. Chem. 47 (1904) 56–102.
[37] N. Wang, T. Tong, M. Xie, J.-F. Gaillard, Lifetime and dissolution kinetics of zinc oxide nanoparticles in aqueous media. Nanotechnology 27 (2016) 324001.
[38] L. Lindfors, P. Skantze, U. Skantze, J. Westergren, U. Olsson, Amorphous drug nanosuspensions. 3. Particle dissolution and crystal growth. Langmuir 23 (2007) 9866–9874.
[39] A.W. Hixson, J.H. Crowell, Dependence of reaction velocity upon surface and agitation. I — Theoretical consideration. Ind. Eng. Chem. 23 (1931) 923–931.
[40] D.R. Ely, R.E. García, M. Thommes, Ostwald–Freundlich diffusion-limited dissolution kinetics of nanoparticles. Powder Technol. 257 (2014) 120–123.

[41] S.-W. Bian, I.A. Mudunkotuwa, T. Rupasinghe, V.H. Grassian, Aggregation and dissolution of 4 nm ZnO nanoparticles in aqueous environments: Influence of pH, ionic strength, size, and adsorption of humic acid. Langmuir 27 (2011) 6059–6068.

[42] D.J. Wesolowski, P. Bénézeth, D.A. Palmer, ZnO solubility and Zn^{2+} complexation by chloride and sulfate in acidic solutions to 290°C with in-situ pH measurement. Geochim. Cosmochim. Acta 62 (1998) 971–984.

[43] C.M. Hudgins, Solubility and density studies of the $CaCl_2$–$ZnCl_2$–H_2O system at 0° and 25°C. J. Chem. Eng. Data 9 (1964) 434–436.

[44] A. Adrover, A. Velardo, M. Giona, S. Cerbelli, F. Pagnanelli, L. Toro, Structural modeling for the dissolution of non-porous ores: Dissolution with sporulation. Chem. Eng. J. 99 (2004) 89–104.

[45] R.J. Seager, A.J. Acevedo, F. Spill, M.H. Zaman, Solid dissolution in a fluid solvent is characterized by the interplay of surface area-dependent diffusion and physical fragmentation. Sci. Rep. 8 (2018) 7711.

[46] H. Cao, D. Karampalis, Y. Li, J. Caragay, A. Alexiadis, Z. Zhang, P.J. Fryer, S. Bakalis, Abrupt disintegration of highly porous particles in early stage dissolution. Powder Technol. 333 (2018) 394–403.

[47] G. Madras, B.J. McCoy, Reversible crystal growth–dissolution and aggregation–breakage: numerical and moment solutions for population balance equations. Powder Technol. 143–144 (2004) 297–307.

[48] Q. Yuan, X. Jia, R.A. Williams, Validation of a multi-component digital dissolution model for irregular particles. Powder Technol. 240 (2013) 25–30.

[49] B. Zhang, C.N. Coon, The relationship of calcium intake, source, size, solubility in vitro and in vivo, and gizzard limestone retention in laying hens. Poult. Sci. 76 (1997) 1702–1706.

[50] D.J. McClements, H. Xiao, P. Demokritou, Physicochemical and colloidal aspects of food matrix effects on gastrointestinal fate of ingested inorganic nanoparticles. Adv. Colloid Interface Sci. 246 (2017) 165–180.

SUPPLEMENTARY MATERIAL

DISSOLUTION KINETICS OF ZINC OXIDE AND ITS RELATIONSHIP WITH PHYSICOCHEMICAL CHARACTERISTICS

Denise Cardoso,[a,b,c] Agnès Narcy,[b] Stéphane Durosoy,[c] Claire Bordes,[a] Yves Chevalier [a,*]

[a] University of Lyon, *LAGEPP, CNRS UMR 5007, Université Lyon 1, 43 bd 11 Novembre, 69622 Villeurbanne, France.*
[b] INRA, *UR 83 Recherches Avicoles, 37380 Nouzilly, France.*
[c] Animine, *10 rue Léon Rey-Grange, 74960 Annecy, France.*

1. Physicochemical characterization of ZnO samples

Clear-cut assessment of complex structures is a difficult task because the various tools for structural investigation do not provide definite measurement of each size. Methods for size measurements are optical and electron microscopies, light scattering and X-ray diffraction. Nitrogen adsorption measurements known as the BET method provide the specific surface area of the powder together with pieces of information on its porosity. Finally, bulk density and tapped density of the dry powder provide an indirect assessment of the formation of aggregates and agglomerates. The experimental results coming from these methods are presented in the following.

Crystalline structure and size of crystallites

All ZnO powders were crystalline under the zincite structure of Wurtzite hexagonal structure of (space group $P6_3mc$) according to the JCPDS database (card No.00-005-0664) (Figure S1).

There are a few methods that can be used to measure the size of primary particles depending on their size-range such as: X-ray diffraction (XRD), TEM and Optical Microscopy. XRD confirmed the same chemical composition and crystallographic structure of all samples. The mean crystallite size D was estimated using the Debye–Scherrer equation:

$$D = 0.9\,\lambda / \beta \cos\theta \qquad \text{(S1)}$$

where λ is the wavelength of the X-ray radiation (0.154 nm), θ and β are the diffraction angle and the resolution-corrected width at half height of Bragg reflections. As the angular resolution of the instrument was 0.055 °, the determination of crystal size was limited to crystals smaller than 100 nm.

Such analysis did not allow an estimate of crystal size for the whole dataset because some samples had crystal size larger than 100 nm. In addition, primary particles may contain several crystals. So, Scherrer analysis of crystal size based on XRD was discarded from the dataset aiming at a statistical analysis of relationships between structure and dissolution kinetics.

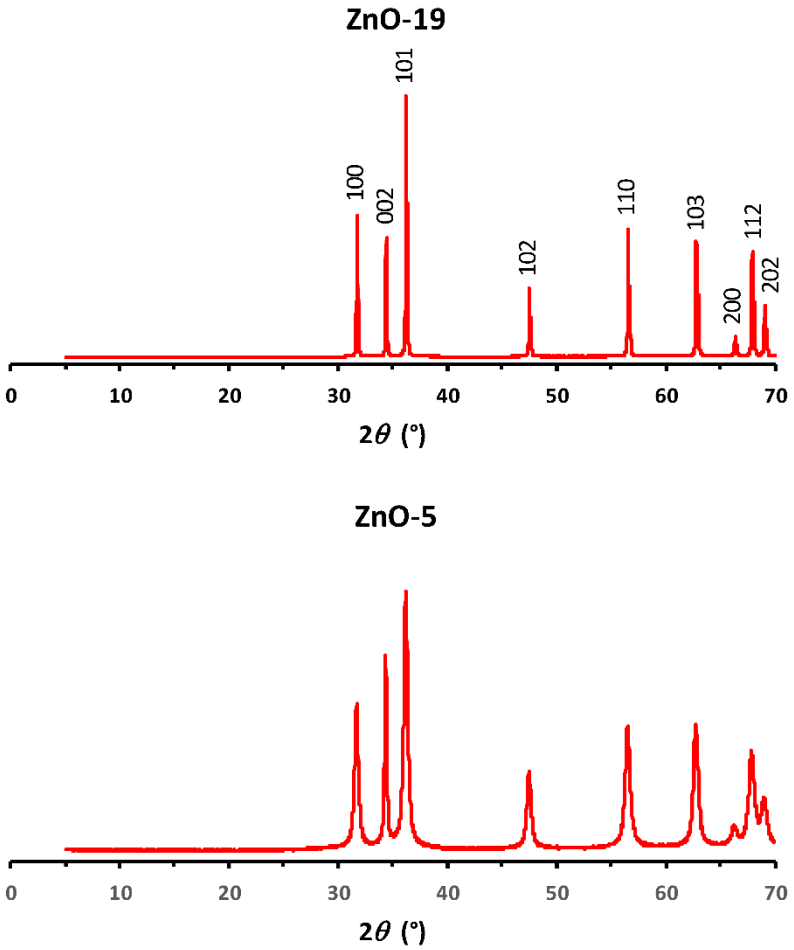

Figure S1. X-ray diffraction powder patterns of ZnO-19 having sharp Bragg reflections (large crystallites) and ZnO-5 with broad Bragg peaks (small crystallites). Miller indices are given on the pattern of ZnO-19.

TEM images can be used to assess the mean size of primary particles from size measurements of a large collection of particles. But it was not possible to observe a large enough number of particles for reaching a relevant statistical average when samples made of large primary particles. Furthermore, when particle shapes are platelets or rods (needles), they tend to lay flat on the surface of the TEM grid they are deposited on, and only the largest dimension can be visualized on the two-dimensional images [1]. Optical microscopy is the most appropriate method to measure the size of large crystals, but it cannot be applied for small-sized particles. Owing to the large differences of primary particle sizes between samples and the impossibility to use a unique technique to measure such size, this parameter was excluded from the analysis. The specific surface area was taken as a better compromise parameter related to the average primary particle size, as a decrease in particle size results in an increase of A_{sp} [2].

Primary particle shape

Morphology of ZnO particles is very sensitive to preparation conditions and methods [3,4]. Typical SEM and TEM pictures shown in Fig. 1 illustrate the different properties among samples. Shape varied from nano to micro-sized platelets, rod-like particles and needles. Some samples contain mixed types of particles. Samples of Fig. 1A,C,D showed to be platelet-shaped, whereas those of Fig. 1B presented a rod-like shape with some presence of needles. Studies of cytotoxicity did not disclose an effect of morphology (shape) on dissolution kinetics of ZnO because aggregation of nanoparticles had a predominant contribution to dissolution [5]. Nevertheless, Heng *et al*. [6] found that differentially shaped ZnO had different dissolution rates, especially spheres and platelets. It is still controversial the effect of shape on dissolution behavior of powders. In the present study, no correlations were observed in relation to the shape. Shape could not be included in the statistical analysis because the shape remains a parameter of descriptive better than quantitative nature.

Aggregate and agglomerate sizes

Although TEM pictures allow observation of shapes and sizes of primary particles, their aggregation and agglomeration observed in the pictures can be a bias, because they can be caused by the drying process for sample preparation [1]. Aggregate and agglomerate sizes were measured by small-angle light scattering. This technique is preferred to methods relying on image analysis because the large number of measured particles provides a nice statistical average of the size [1]. Due to dry powders properties, particle size distribution can be influenced in many ways; therefore setting the materials sampling methodology for measuring is very important [7]. The size of agglomerates was measured by a mild dispersion of ZnO powder in water that did not break agglomerates. The ratio of agglomerates to aggregates sizes was called ‘agglomeration ratio’.

Primary particles sizes roughly estimated from TEM images were smaller than sizes coming from small-angle light scattering measurements, as has already been noticed by Peng *et al*. [5]. Small nanoparticles with a large A_{sp} tend to aggregate and form micro-sized particles in aqueous environment [6,8]. The present nanoparticles observed in TEM images appeared assembled as submicron-size aggregates and agglomerates.

Specific surface area and porosity

Specific surface area (A_{sp}) has been measured by the BET method. It aims at assessing the surface exposure of a particle to the liquid medium. A_{sp} is associated to primary particle size since aggregation does not decrease A_{sp}. The nitrogen adsorption isotherms were of different types. For some samples, adsorption and desorption isotherms were superimposed, showing that samples did not have porosity (Fig. 2a). Conversely adsorption and desorption isotherms showed the classical type IV adsorption isotherm suggesting the presence of a mesoporous structure (Fig. 2b). At high relative pressure from 0.45 to 0.80, such isotherms exhibited a hysteresis loop of type H2, indicating the existence of pores with narrow necks and wide bodies.

The specific surface area A_{sp} was calculated in the classical way by fitting the theoretical BET isotherm, Eq. (S2), to experimental data between relative pressures p/p_0 = 0.05 and 0.3.

$$\frac{p}{V(p_0-p)} = \frac{1}{V_m c} + \frac{c-1}{V_m c}\frac{p}{p_0} \quad \text{(S2)}$$

where V_m is the volume of nitrogen adsorbed in the first layer at full coverage in direct contact to the solid surface and c is the BET constant related to the difference of adsorption energy of nitrogen to the bare surface and to a layer of already adsorbed nitrogen molecules. A_{sp} was calculated from V_m taking the molecular area of a nitrogen molecule as 16.2 Å^2.

For mesoporous samples, the pore size distribution was calculated from the desorption branch of the isotherm by the BJH method [9] using the Kelvin equation (Eq. (S3)) and Eq. (S4) for the reference non-porous material.

$$\ln\left(\frac{p}{p_0}\right) = \frac{2\gamma v_{mol}\cos\theta}{R_K RT} \quad \text{(S3)}$$

where v_{mol} is the molar volume of liquid nitrogen (v_{mol} = 34.67 cm^3·mol^{-1}) and γ is the surface tension of liquid nitrogen (γ = 8.85 mN·m^{-1}). Total wetting of the solid surface by liquid nitrogen is assumed, so that the contact angle was θ = 0 °.

The diameter of the pores, D, is twice the sum of the radius given by the Kelvin equation and the thickness of the adsorbed layer of nitrogen to the reference non-porous material given by $\boldsymbol{t(\mathrm{nm}) = 0.354\ \frac{V}{V_m}}$.

The adsorption isotherm of the hypothetic reference non-porous material according to BJH is

$$\frac{V}{V_m} = \left[\frac{-5}{ln(p/p_0)}\right]^{1/3} \quad \text{(S4)}$$

The difference between the experimental nitrogen volume and the BJH non-porous reference is the porous volume.

Some ZnO powders show adsorption isotherms with no hysteresis at nitrogen gas desorption (Fig. S2A) while others show definite hysteresis (Fig. S2B) revealing mesoporous structure of the powder. The BJH method allowed the calculation of the distribution of mesoporous volume in case of mesoporous samples (inset of Fig. S2B). Very low porous volume below significance was derived in case of non-porous samples (inset of Fig. S2A).

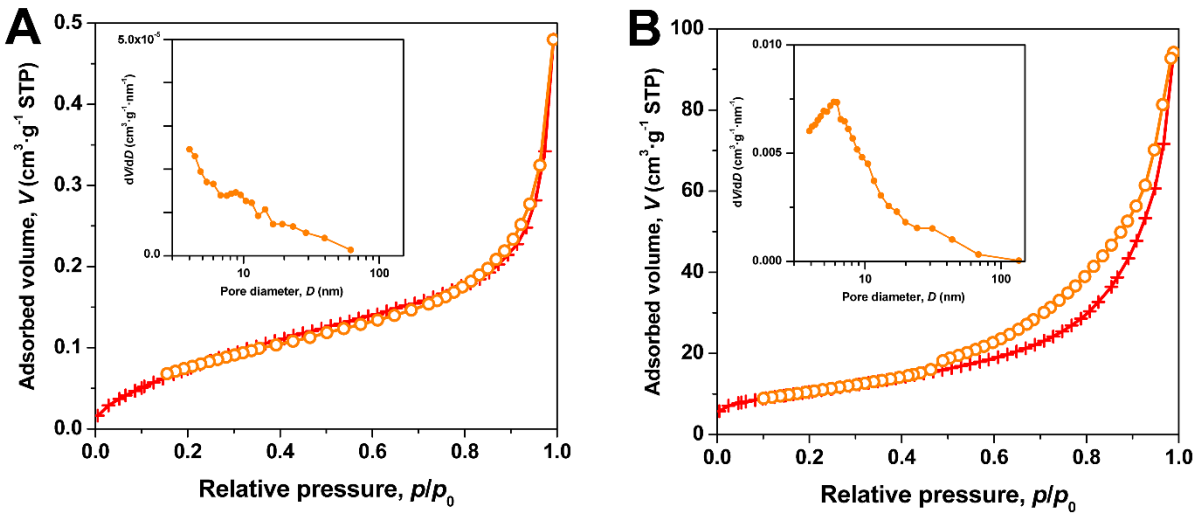

Figure S2. BET adsorption isotherms showing the adsorption (+) and desorption (○) branches of ZnO-6 (A) that does not show hysteresis and ZnO-4 (B) having mesoporosity. Insets show the distribution of mesoporous volume d*V*/d*D* calculated by the BJH method. Notice the different vertical scales of insets in parts A and B.

The specific area results are summarized in Table 1. The smallest A_{sp} that can be measured by the BET method was 0.1 $m^2 \cdot g^{-1}$. Sample ZnO-20 that its A_{sp} is marked 0.0 $m^2 \cdot g^{-1}$ in Table 1 has actually A_{sp} lower than the BET measurement limit of 0.1 $m^2 \cdot g^{-1}$. ZnO samples of type D in Fig. 1 showed the largest A_{sp} values reaching up to 41 $m^2 \cdot g^{-1}$. Samples of type A had the lowest A_{sp} values of less than 0.1 to 0.5 $m^2 \cdot g^{-1}$. Those of types B and C showed variable A_{sp}. High values of A_{sp} are often thought being associated to a faster dissolution, as greater area of contact between the particle surface and aqueous solution is facilitating dissolution.

The mean pore size was estimated from the pore size distribution of porous volume d*V*/d*D* as a $D_{pore}(0.5)$ defined in the same way as for a particle size distribution: half the porous volume is inside pores smaller than $D_{pore}(0.5)$. There were many samples which did not show hysteresis behavior characteristic of mesoporosity, so that measurements of pore volume and size could not be included in the statistical analysis. The median pore size $D_{pore}(0.5)$ of mesoporous powders was close to crystallite size, provided they are lower than 100 nm (Fig. S3A). Such identity of sizes suggests that porosity corresponds to interstices between particles. In such a case, primary particles are made of a single crystal. Their porous volume was also correlated with crystallite size (Fig. S3B). Large porous volume was obtained with powders made of small crystals associated as loose aggregates/agglomerates. Such correlations no longer held for non-porous powders that several of them had small crystallite sizes and vanishingly small porous volume. A rationale to such observation is that mesoporosity requires small particles. Powders made of small crystals can be non-porous in cases where they are stuck together as dense aggregates of large size as revealed by TEM.

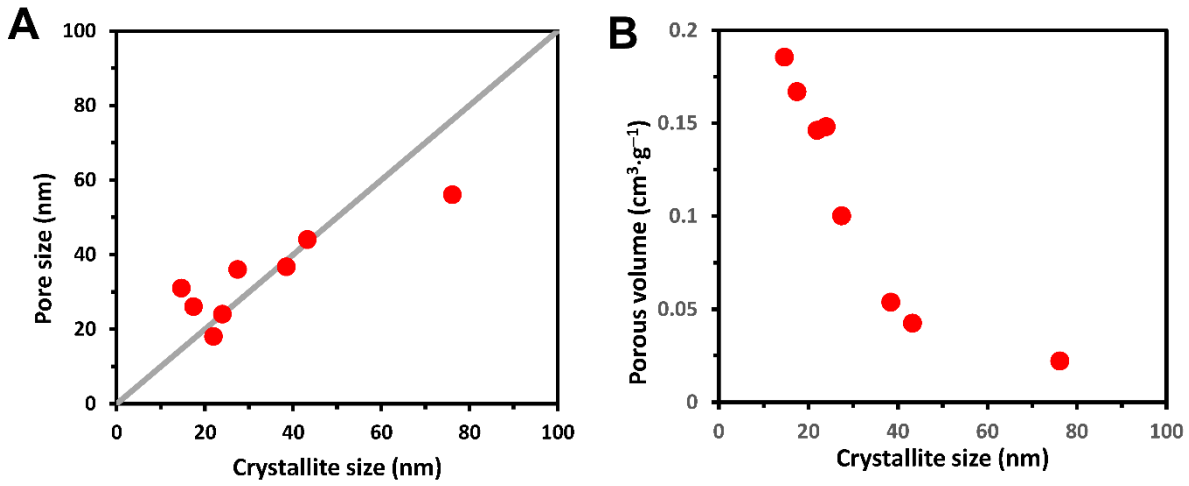

Figure S3. (A) Correlation between pore size and crystallite size. The diagonal line corresponds to equality of them. (B) Correlation between porous volume and crystallite size. All these powders have crystallite size smaller than 100 nm.

Bulk density, tapped density and Hausner ratio

Bulk density of dry powders is the ratio of mass by the volume occupied by the powder. Low densities are associated to loose aerated aggregates and/or agglomerates of particles stuck together during the fabrication and/or drying processes. Sticking by means of sintering is irreversible; it causes formation of unbreakable aggregates. Agglomerates are formed by association of aggregates through bonds coming from interparticle forces of various types like dispersion, polar or hydrogen-bonding ones; they can be broken into aggregates by mechanical stirring during the dispersion process in aqueous medium. With regards to the structure of ZnO particles, density of the dry powder provides an indirect estimate of the extent of aggregation and agglomeration. This qualitative relationship is in agreement with the present findings. The lowest density values were related to aggregates/agglomerates with small size of primary particles. Conversely, particles of large size and rounded shape can pile up as more compact powders of high density [10].

Tapped density is measured after tapping the container holding the aerated sample following the ISO 8398 standard. Powder particles are forced to rearrange to close contact upon tapping. Tapped density is the densest the powder can achieve under a moderate compression stress. Tapping erases the memory of the last stages of the manufacture process, mainly drying and final manipulations. The tapped density better characterizes particles packing under the control of interparticle interactions in dry medium. Hausner ratio is tapped density over bulk density; it is a useful tool to define cohesion of a powder [10,11]. The lower this ratio, the less cohesive is the powder, meaning the lower tendency for further consolidation. The interparticle forces causing powder cohesion are stronger for small primary particle sizes [12].

The lowest variation observed was 5 % of volume reduction from density to tapped density. When the powder is given mobility through tapping, large and small particles are able to

rearrange. As most of the small particles migrate to the bottom between the largest, the highest volume variation of samples observed was 40 % for samples composed of mixed fine powders and big clusters that, once tapped, adjust to the container when small particles migrate into interstices between large ones [10].

References

[1] K.W. Powers, M. Palazuelos, B.M. Moudgil, S.M. Roberts, Characterization of the size, shape, and state of dispersion of nanoparticles for toxicological studies. Nanotoxicology 1 (2007) 42–51.

[2] M. Mosharraf, C. Nyström, The effect of particle size and shape on the surface specific dissolution rate of microsized practically insoluble drugs. Int. J. Pharm. 122 (1995) 35–47.

[3] A. Moezzi, A. McDonagh, M. Cortie, Zinc oxide particles: synthesis, properties and applications. Chem. Eng. J. 185 (2012) 1–22.

[4] D. Li, H. Haneda, Morphologies of zinc oxide particles and their effects on photocatalysis. Chemosphere 51 (2003) 129–137.

[5] X. Peng, S. Palma, N.S. Fisher, S.S. Wong, Effect of morphology of ZnO nanostructures on their toxicity to marine algae. Aquatic Toxicol. 102 (2011) 186–196.

[6] B.C. Heng, X. Zhao, E.C. Tan, N. Khamis, A. Assodani, S. Xiong, C. Ruedl, K.W. Ng, J.S. Loo, Evaluation of the cytotoxic and inflammatory potential of differentially shaped zinc oxide nanoparticles. Arch. Toxicol. 85 (2011) 1517–1528.

[7] R. Marsalek, Particle size and zeta potential of ZnO. APCBEE Procedia 9 (2014) 13–17.

[8] C.A. David, J. Galceran, C. Rey-Castro, J. Puy, E. Companys, J. Salvador, J. Monné, R. Wallace, A. Vakourov, Dissolution kinetics and solubility of ZnO nanoparticles followed by AGNES. J. Phys. Chem. C 116 (2012) 11758–11767.

[9] S. Lowell, J.E. Shields, M.A. Thomas, M. Thommes, Characterization of Porous Solids and Powders: Surface Area, Pore Size and Density. Kluwer, Dordrecht, 2004, vol. 8, pp. 101–128.

[10] E.C. Abdullah, D. Geldart, The use of bulk density measurements as flowability indicators. Powder Technol. 102 (1999) 151–165.

[11] M. Leturia, M. Benali, S. Lagarde, I. Ronga, K. Saleh, Characterization of flow properties of cohesive powders: A comparative study of traditional and new testing methods. Powder Technol. 253 (2014) 406–423.

[12] M.E. Aulton, K.M.G. Taylor, Aulton's Pharmaceutics: The Design and Manufacture of Medicines. 4th edition, Churchill Livingstone Elsevier, Edinburgh, 2013.